

Z' production at the LHC in the four-site Higgsless model

Elena Accomando^(a), Stefania De Curtis^(b), Daniele Dominici^(b,c) and Luca Fedeli^(b,c)

(a) *NExT Institute and School of Physics and Astronomy,
University of Southampton, Highfield, Southampton SO17 1BJ, UK*

(b) *INFN, 50019 Sesto F., Firenze, Italy*

(c) *Department of Physics, University of Florence, 50019 Sesto F., Firenze, Italy.*

We study the phenomenology of the neutral gauge sector of the four-site Higgsless model, based on the $SU(2)_L \times SU(2)_1 \times SU(2)_2 \times U(1)_Y$ gauge symmetry, at present colliders. The model predicts the existence of two neutral and four charged extra gauge bosons, $Z_{1,2}$ and $W_{1,2}^\pm$. We expand and update a previous study, by concentrating on the neutral sector. We derive new limits on $Z_{1,2}$ -boson masses and couplings from recent direct searches at the Tevatron. We moreover estimate the discovery potential at the Tevatron with a project luminosity $L=10 \text{ fb}^{-1}$, and at the 7 TeV LHC with $L=1 \text{ fb}^{-1}$.

In contrast to other Higgsless theories characterized by almost fermiophobic extra gauge bosons, the four-site model allows sizeable $Z_{1,2}$ -boson couplings to SM fermions. Owing to this feature, we find that in the next two years the extra $Z_{1,2}$ -bosons could be discovered in the favoured Drell-Yan channel at the 7 TeV LHC for $Z_{1,2}$ masses in the TeV region, depending on model parameters.

I. INTRODUCTION

Models with additional extra-dimensions [1–4] have received, during the last ten years, considerable attention because they are a new interesting attempt to explain the large difference between the Planck scale and the Fermi scale via geometrical arguments. They also provide new mechanisms of electroweak symmetry breaking (EWSB). The symmetry could in fact be broken either by orbifolding or via boundary conditions on the compact extra dimensions. As a consequence, a remarkable activity has been devoted to investigate Higgsless Models (HM) [5–9]. HM, being 5D gauge models, predict the existence of new Kaluza-Klein (KK) vector resonances, which help in delaying the unitarity violation of vector boson scat-

tering (VBS) amplitudes to higher energies, compared to the corresponding scale of the Standard Model (SM) without a light Higgs [5, 10]. The discretization of the compact fifth dimension, over which HM are defined, generates the so-called deconstructed theories which are described by 4D chiral lagrangians with a number of replicas of the gauge group equal to the number of lattice sites [11–19]. The main difficulty for all these models, as for technicolor theories, is to reconcile the presence of a relatively low KK-spectrum, necessary to delay the unitarity violation to TeV-energies, with the electroweak precision tests (EWPT) whose measurements are in very good agreement with SM predictions. One possible solution is obtained by either delocalizing fermions along the fifth dimension [20, 21] or, equivalently in the deconstructed picture, by allowing for direct couplings between new vector bosons and SM fermions [22]. In the simplest version of this latter class of models, corresponding to just three lattice sites and gauge symmetry $SU(2)_L \times SU(2) \times U(1)_Y$ (the so-called BESS model [23, 24]), the requirement of vanishing of the $\epsilon_3(S)$ parameter implies that the new triplet of vector bosons is almost fermiophobic; then the only production channels for their search are those driven by boson-boson couplings. The HM literature has been thus mostly focused on difficult multi-particle processes which require high luminosity to be detected, that is vector boson fusion and associated production of new gauge bosons with SM ones [25–29].

In a recent paper [30], we have considered the generalization of the minimal three-site model by inserting an additional lattice site. The four-site Higgsless model, which emerges, is based on the $SU(2)_L \times SU(2)_1 \times SU(2)_2 \times U(1)_Y$ gauge symmetry and predicts two neutral and four charged extra gauge bosons, $Z_{1,2}$ and $W_{1,2}^\pm$. Its novelty and strenght consist in satisfying EWPT constraints without imposing the new resonances to be fermiophobic. Within this framework, the favoured Drell-Yan channel becomes particularly relevant for the extra gauge boson search at the LHC [30–32] and the upgraded Tevatron.

Aim of this paper is to update the phenomenological aspects of the KK neutral sector, studied in [30, 31], by taking into account recent data from Tevatron and the new plans of the 7 TeV LHC. We compare the sensitivity reach of the Tevatron with 10 fb^{-1} of integrated luminosity and the LHC at 7 TeV with $L=1 \text{ fb}^{-1}$. We also study how the sensitivity reach could improve at the 14 TeV LHC with $L=10 \text{ fb}^{-1}$.

The paper is organized as follows. In Section II, we briefly review the model. In Section III, we discuss mass spectrum, decay widths and branching ratios of the two additional

neutral bosons. In Section IV, we perform a detailed analysis of $Z_{1,2}$ Drell-Yan cross-sections and invariant mass distributions. We compare the results expected in the next two years at the Tevatron with $L=10 \text{ fb}^{-1}$ and the 7 TeV LHC with $L=1 \text{ fb}^{-1}$, with those ones reachable at the upgraded 14 TeV LHC with $L=10 \text{ fb}^{-1}$. In Section V, we derive exclusion limits on the $Z_{1,2}$ bosons from Tevatron and LHC experiments, and we discuss their discovery prospects. Conclusions are given in Section VI. In Appendix A, we list all relevant trilinear gauge boson couplings.

II. THE MODEL: UNITARITY AND EWPT BOUNDS

The class of models, we are interested in, is described by a chiral Lagrangian based on the $SU(2)_L \otimes SU(2)^K \otimes U(1)_Y$ gauge symmetry and $K + 1$ non linear σ -model scalar fields Σ_i , interacting with the gauge fields. The K gauge coupling constants, g_i , and the $K + 1$ link couplings, f_i , define the free parameters of the model beyond the SM ones. Different f_i , in the continuum limit, can describe a generic metric [18, 21, 22, 33, 34]. The flat metric corresponds to constant link couplings: $f_i = f_c (i = 1, K + 1)$. $SU(2)_L$ and $U(1)_Y$ gauge symmetries act on the two ends of the linear moose, which in the continuum become the boundaries of the fifth dimension. Standard fermions are localized on those ends and do not interact with the internal gauge bosons. However, direct couplings between SM fermions and new gauge bosons can be included in a way that preserves the symmetry of the model. This can be achieved either by considering composite operators [22–24] or via a mixing with new heavy fermions interacting with the new gauge bosons [35]. We consider only direct couplings between new gauge bosons and left-handed SM fermions, with strength given by the K dimensionless parameters b_i . The case $K = 1$ corresponds to the BESS model [23, 24] with a particular choice of the parameters. Here, we concentrate on the case $K = 2$ which in turn corresponds to a specific choice of the parameters of the vector and axial vector-extension of the BESS model [36]. For simplicity, we assume $g_2 = g_1$ and $f_3 = f_1$. This choice leads to a Left-Right symmetry in the new gauge sector, giving rise to a definite parity for the corresponding gauge bosons once the standard gauge interactions are turned off. Summarizing, the four-site Higgsless model has five parameters a priori: g_1, f_1, f_2, b_1 and b_2 . However, this number gets reduced to three by phenomenological constraints as discussed in the following.

Charged and neutral gauge boson spectrum and couplings to SM fermions are given in [30, 31] by means of a perturbative expansion in series of $x^2 = \tilde{g}^2/g_1^2$. Neutral non zero mass eigenvalues have the following expressions, up to $\mathcal{O}(x^4)$:

$$M_Z^2 = \tilde{M}_Z^2 (1 - x^2 z_Z) \quad (1)$$

$$M_{Z_1}^2 = M_1^2 \left(1 + \frac{x^2}{2c_{\tilde{\theta}}^2} \right) \quad (2)$$

$$M_{Z_2}^2 = M_2^2 \left(1 + \frac{x^2 z^2}{2c_{\tilde{\theta}}^2} \right) \quad (3)$$

where

$$\tilde{M}_Z^2 = \frac{\tilde{M}_W^2}{c_{\tilde{\theta}}^2}, \quad \tilde{M}_W^2 = \tilde{g}^2 v^2 / 4, \quad z_Z = \frac{1}{2} \frac{(z^4 + c_{2\tilde{\theta}}^2)}{c_{\tilde{\theta}}^2} \quad (4)$$

$$M_1^2 = f_1^2 g_1^2, \quad M_2^2 = g_1^2 (f_1^2 + 2f_2^2), \quad z = M_1/M_2 < 1 \quad \text{and} \quad t_{\tilde{\theta}} = s_{\tilde{\theta}}/c_{\tilde{\theta}} \quad (5)$$

In the mass eigenstate basis, the Lagrangian describing the neutral fermion-boson interaction is given by:

$$\mathcal{L}_{NC} = \bar{\psi} \gamma^\mu \left[-e \mathbf{Q}_f A_\mu + (a_{ZL}^f P_L + a_{ZR}^f P_R) Z_\mu + (a_{1L}^f P_L + a_{1R}^f P_R) Z_{1\mu} + (a_{2L}^f P_L + a_{2R}^f P_R) Z_{2\mu} \right] \psi \quad (6)$$

where $P_{L,R} = (1 \mp \gamma_5)/2$ and $a_{ZL(R)}^f, a_{1,2L(R)}^f$ are the left-handed (right-handed) couplings of $Z, Z_{1,2}$ bosons to SM fermions respectively. Their explicit expressions are given by [30]

$$a_{ZL}^f = -\frac{\tilde{g}}{c_{\tilde{\theta}}} \left(1 - \frac{b}{2} \right) \left(1 - x^2 \frac{z_Z}{2} \right) \left[\frac{\tau_3^f}{2} - \frac{s_{\tilde{\theta}}^2}{1 - \frac{b}{2}} \left(1 - x^2 \frac{c_{\tilde{\theta}}}{s_{\tilde{\theta}}} z_{Z\gamma} \right) Q^f \right] \quad (7)$$

$$a_{ZR}^f = \frac{\tilde{g}}{c_{\tilde{\theta}}} \left(1 - \frac{b}{2} \right) \left(1 - x^2 \frac{z_Z}{2} \right) \left[\frac{s_{\tilde{\theta}}^2}{1 - \frac{b}{2}} \left(1 - x^2 \frac{c_{\tilde{\theta}}}{s_{\tilde{\theta}}} z_{Z\gamma} \right) Q^f \right] \quad (8)$$

$$a_{1L}^f = -\frac{\tilde{g}x}{\sqrt{2}(1+b_+)} \left(\frac{b_+}{x^2} - \frac{c_{2\tilde{\theta}}}{c_{\tilde{\theta}}^2} \right) \frac{\tau_3^f}{2} + \frac{\tilde{g}x t_{\tilde{\theta}}^2}{\sqrt{2}} Q^f \quad (9)$$

$$a_{1R}^f = \frac{\tilde{g}x t_{\tilde{\theta}}^2}{\sqrt{2}} Q^f \quad (10)$$

$$a_{2L}^f = -\frac{\tilde{g}x}{\sqrt{2}(1+b_+)} \left(\frac{b_-}{x^2} - \frac{z^2}{c_{\tilde{\theta}}^2} \right) \frac{\tau_3^f}{2} - \frac{\tilde{g}x z^2 t_{\tilde{\theta}}^2}{\sqrt{2}} Q^f \quad (11)$$

$$a_{2R}^f = -\frac{\tilde{g}x z^2 t_{\tilde{\theta}}^2}{\sqrt{2}} Q^f \quad (12)$$

where

$$z_{Z\gamma} = -t_{\tilde{\theta}}c_{2\tilde{\theta}} \quad b = \frac{b_+ - b_-z^2}{(1 + b_+)} \quad b_{\pm} = b_1 \pm b_2 \quad (13)$$

Q^f is the electric charge in unit e (the proton charge). In the following we will factorize out the electric charge by defining $a_{iL,R}^f = -e\hat{a}_{iL,R}^f$, $i = 1, 2$.

Using these equations, we can rewrite the free parameters of the four-site model in terms of observable quantities. The physical $Z_{1,2}$ -boson masses, M_{Z_1, Z_2} , are indeed closely related to $f_{1,2}$ as shown in Eqs. (2-5). Moreover, the $Z_{1,2}$ -boson couplings to SM fermions, \hat{a}_{1L}^f and \hat{a}_{2L}^f , are unique functions of $b_{1,2}$ once g_1 , M_{Z_1, Z_2} are fixed. We can then recast the free parameter set $(g_1, f_1, f_2, b_1, b_2)$ previously given into $(g_1, M_{Z_1}, M_{Z_2}, \hat{a}_{1L}^e, \hat{a}_{2L}^e)$. Having everything expressed in terms of physical quantities, we are now ready to discuss the phenomenological constraints.

We get a first relation among the newly defined parameters of the model by imposing the SM gauge boson masses to have the measured values. Namely we get at the leading order:

$$x \sim \frac{M_W}{M_1} \sqrt{\frac{2}{1-z^2}} \sim \frac{c_{\tilde{\theta}} M_Z}{M_1} \sqrt{\frac{2}{1-z^2}} \quad (14)$$

This reduces the number of independent parameters by unit as $g_1 = g_1(M_{Z_1}, M_{Z_2}, \hat{a}_{1L}^f, \hat{a}_{2L}^f)$.

In addition, the abovementioned relation has an important consequence on the allowed spectrum for the new $Z_{1,2}$ gauge bosons. Since mass eigenvalues and eigenvectors have been computed via an analytical expansion in the x -variable, in Fig. 1 (left panel) we plot the validity range of this approximation. The dashed-line contour corresponds to $x^4 = 5 \times 10^{-3}$, and defines the minimum Z_2 -boson mass allowed by the model (at leading order) as a function of the free parameter z . Hence, being z the ratio between Z_1 and Z_2 -boson masses, a lower bound on the global mass spectrum is established. In the following we will refer to this bound as the approximation limit. Next we remind that, owing to the exchange of the extra gauge bosons, the perturbative unitarity violation of the longitudinal vector boson scattering amplitudes with purely SM external bosons (including all external gauge bosons) can be delayed up to $\sqrt{s} = 5(3)\text{TeV}$ [30, 31]. This condition gives an upper bound on the mass spectrum of the new particles, which are thus constrained to be between few hundreds GeV and few TeV as displayed in Fig. 1 (left panel).

In general, the only way to combine the need of relatively light extra gauge bosons with EWPT is to impose the new particles to be fermiophobic. In the four-site Higgsless model, this strong assumption is not necessary anymore. In order to show this feature, we compute

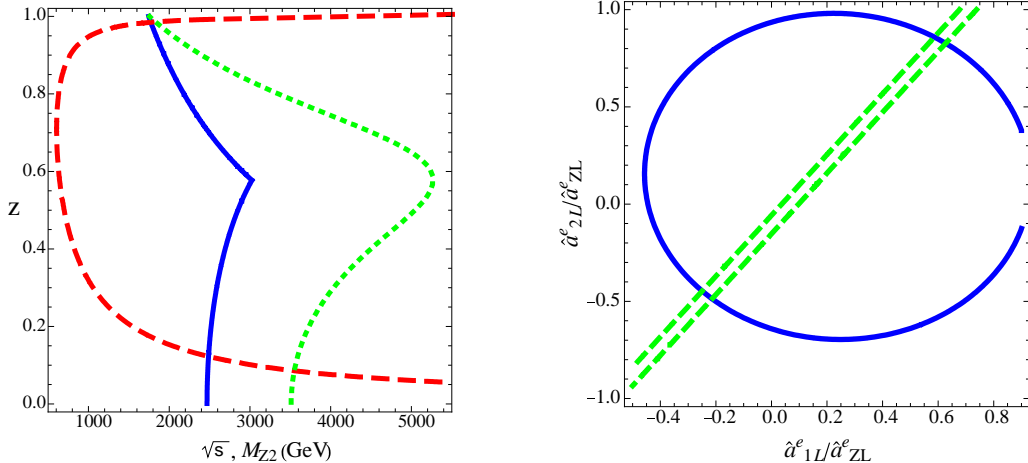


FIG. 1: Left: Unitarity bounds on the plane (\sqrt{s}, z) coming from Vector Boson Scattering (VBS) amplitudes with purely SM bosons in the external legs (green dot line), and with SM plus extra gauge bosons in the external legs (blue solid line). The allowed regions are on the left of the contours. The red dashed line gives the minimum value of the Z_2 -boson mass spectrum (and accordingly the minimum value of M_{Z_1} which can be derived from z) allowed by the four-site model at leading order (see text). Right: 95% C.L. bounds on the plane $(\hat{a}_{1L}^e/\hat{a}_{ZL}^e, \hat{a}_{2L}^e/\hat{a}_{ZL}^e)$ from ϵ_3 (green dashed line) and ϵ_1 (blue solid line) for $z = 0.8$ and $M_1 = 1$ TeV (corresponding to $M_{Z_1, Z_2} = 1012, 1256$ GeV). The allowed regions are the internal ones.

the new physics contribution to the electroweak parameters ϵ_1 , ϵ_2 and ϵ_3 , including one-loop radiative corrections (they are evaluated within the Higgsless SM for a 1 TeV cutoff). Then we compare the result with the ϵ_i ($i=1,3$) experimental values [37]. For fixed $Z_{1,2}$ -boson masses, one obtains bounds on the two remaining free parameters, which we choose to be \hat{a}_{1L}^e and \hat{a}_{2L}^e , the $Z_{1,2}$ -boson couplings to the left-handed electron. The result is shown in Fig. 1 (right panel) for the sample case: $z = 0.8$ and $M_1 = 1$ TeV corresponding to $(M_{Z_1, Z_2} = 1012, 1256$ GeV). No bound comes from ϵ_2 thanks to its negative experimental value. The ϵ_1 parameter gives weak limits on the magnitude of the $Z_{1,2}$ boson-electron couplings. As a consequence, they are free to be of the order of the SM ones. This clearly shows that, oppositely to most common Higgsless theories present in the literature, the four-site model is not-fermiophobic at all and could be probed in the favoured Drell-Yan channel already at the LHC start-up.

The real EWPT constraint comes from the ϵ_3 parameter, which imposes a strict relation

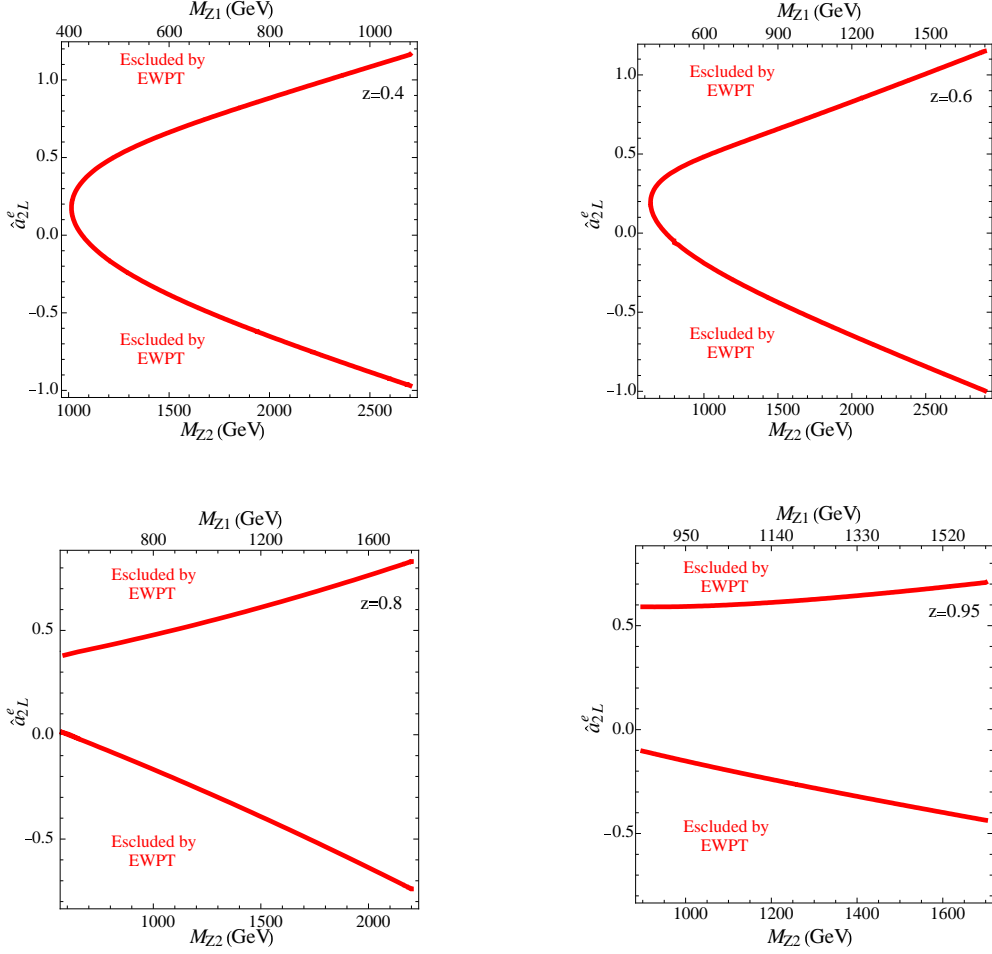


FIG. 2: 95% C.L. EWPT bounds in the plane $(M_{Z_2}, \hat{a}_{2L}^e)$. The allowed region is inside the thick red curve; lower and upper values for M_{Z_2} come respectively from approximation and unitarity limits (see Fig. 1). The four plots refer to four different values of the free z -parameter: $z=0.4$ (top-left), $z=0.6$ (top-right), $z=0.8$ (bottom-left), $z=0.95$ (bottom-right).

between \hat{a}_{1L}^e and \hat{a}_{2L}^e , as displayed by the dashed-line contour in Fig. 1 (right panel) where the band width is due to the experimental error on ϵ_3 . This strong bound allows one to derive a second relation between the free parameters of the model. Assuming ϵ_3 equal to its central value [37]:

$$\epsilon_3 = \frac{\sqrt{2}e}{g_1}(\hat{a}_{1L}^e - z^2\hat{a}_{2L}^e) - \frac{e^2}{g_1^2 c_\theta^2}(1 + z^4) = 4.8 \times 10^{-3} \quad (15)$$

one can write the Z_1 -boson electron coupling, \hat{a}_{1L}^e , as a function of \hat{a}_{2L}^e at fixed $Z_{1,2}$ -boson masses. The net result is that the number of independent free parameters gets further reduced to three. In the next sections, to describe the four-site Higgsless model, we will

choose the following set: $z, M_{Z_2}, \hat{a}_{2L}^e$ (from Eqs.(2),(3),(5) $z = M_1/M_2 = M_{Z_1}/M_{Z_2} + \mathcal{O}(x^2)$). The parameter space allowed by EWPT is shown in Fig. 2 for various values of the free z parameter.

III. EXTRA $Z_{1,2}$ -BOSONS: MASS SPECTRUM, DECAY WIDTHS AND BRANCHING RATIOS

In this section, we summarize the main properties of the heavy $Z_{1,2}$ -bosons. The first peculiarity of the four-site model is related to the nature of the two extra gauge bosons and their mass hierarchy. The lighter particle, Z_1 , is a vector boson while the heavier one, Z_2 , is an axial-vector (neglecting electroweak corrections). Oppositely to closely related models, like the walking technicolor [38], no mass spectrum inversion is possible. The mass splitting, $\Delta M = M_{Z_2} - M_{Z_1}$, is always positive and its size depends on the free z -parameter:

$$\Delta M = (1 - z)M_{Z_2} + \mathcal{O}(x^2) \quad 0 < z < 1. \quad (16)$$

We can thus have scenarios where the two resonances lie quite apart from each other, and portions of the parameter space in which they are (almost) degenerate. In the latter case, the multi-resonance distinctive signature would collapse into the more general single Z' signal. The four-site model would thus manifest a degeneracy with the well known extra U(1) theories predicting only one additional neutral gauge boson. The mass spectrum has both a lower and an upper bound, as discussed in Sect.II. It lies roughly in the range $350 \leq M \leq 3000$ GeV.

The total widths of the two heavy gauge bosons, $\Gamma_{Z_{1,2}}$, are displayed in Fig. 3 as a function of their mass for four values of the z -parameter: $z = 0.4, 0.6, 0.8, 0.95$. They have been computed by taking as $Z_{1,2}f\bar{f}$ couplings those corresponding to the maximal \hat{a}_{2L}^e value allowed by EWPT for each z value (upper lines in Fig. 2). This maximizes the fermionic contribution to the total decay width, and it will be used later to show the maximal branching ratio one might expect for the $Z_{1,2}$ -boson decay into electrons.

From Fig. 3, one can see that both Z_1 and Z_2 are very narrow for low mass values. In the low edge of their spectrum, the magnitude of their total width is around a few GeV. Since the width is dominated by the $Z_{1,2}$ -boson decay into gauge boson pairs (when kinematically allowed) whose behaviour is proportional to $M_{Z_{1,2}}^3$, it then increases with the mass up to

hundreds of GeV. This can be easily seen from the diboson contribution to the total decay widths which, at leading order in the x -parameter given in Eq. (14), have the following expressions

$$\Gamma_{Z_1}^{WW} = \frac{1}{3\pi} \left(\frac{\tilde{g}}{16} \right)^2 \frac{M_{Z_1}^3}{M_W^2} (1 - z^4)(1 + z^2) \quad (17)$$

$$\Gamma_{Z_2}^{W_1W} = \frac{1}{3\pi} \left(\frac{\tilde{g}}{16} \right)^2 \frac{M_{Z_2}^3}{M_W^2} z^4 (1 - z^2)^3 [1 + 10z^2 + z^4]. \quad (18)$$

for the Z_1 and Z_2 bosons, respectively.

Let us briefly comment these formulas. The dependence of $\Gamma_{Z_{1,2}}$ from the z -parameter has a twofold source. It comes partially from the structure of the Z_1WW and Z_2W_1W trilinear couplings (see Appendix A), and in part by the fact that the z -parameter determines whether the $Z_2 \rightarrow W_1W$ channel is kinematically open (the $Z_2 \rightarrow W_1W_1$ channel is suppressed by the coupling). At fixed mass, $\Gamma_{Z_1}^{WW}$ slightly decreases by increasing the z -parameter owing to the self-coupling $a_{WWZ_1} \propto (1 - z^4)$ given in eq. (A4). On the contrary, $\Gamma_{Z_2}^{W_1W}$ gets larger by increasing the z -parameter owing to the trilinear coupling $a_{W_1WZ_2} \propto z^2$ given in eq. (A7). This latter behaviour persists until the growth of the coupling can balance the reduction of the kinematically allowed phase space for producing the W_1W boson pairs. As the z -parameter increases, Z_2 and W_1 become more and more degenerate in mass: $M_{Z_2} \simeq M_{W_1}$. Hence, the phase space shrinks until it gets closed for $z \geq 1 - M_W/M_{Z_2}$. When the $Z_2 \rightarrow W_1W$ channel is kinematically forbidden, the total width is given by the Z_2 -boson decay into fermions. Its size is thus drastically reduced as displayed in Fig. 3 (bottom-right) for $z = 0.95$. The above mentioned combination of coupling and phase space effects explains the $\Gamma_{Z_{1,2}}$ behaviour shown in Fig. 3. From the plots, it is also clear that Z_2 is broader than Z_1 as soon as its decay into boson pairs opens up.

Since the $Z_{1,2}$ total width can range between a few and hundreds GeV, a natural question is whether it would be possible to measure it at the LHC. The mass resolution during the early stage of the LHC is estimated to be $R_{LHC} = 2\%M$ [39–41]. If $0.5 \cdot \Gamma_{Z_{1,2}} \geq R_{LHC}$ (or $\Gamma_{Z_{1,2}}/(2M_{Z_{1,2}}) \geq 2\%$), then the shape of the corresponding resonance could be fully reconstructed and analysed. In this case, the decay width could be measured. In Fig. 4, we show contour plots defining in what region of the parameter space the total width could be in principle measured. The two plots refer to two representative values of the free z -parameter: $z = 0.6, 0.8$. Within the corresponding parameter space, limited by EWPT bounds (thick red lines), the figures contain four contour lines. The blue solid line corresponds to $0.5 \cdot \Gamma_{Z_2} =$

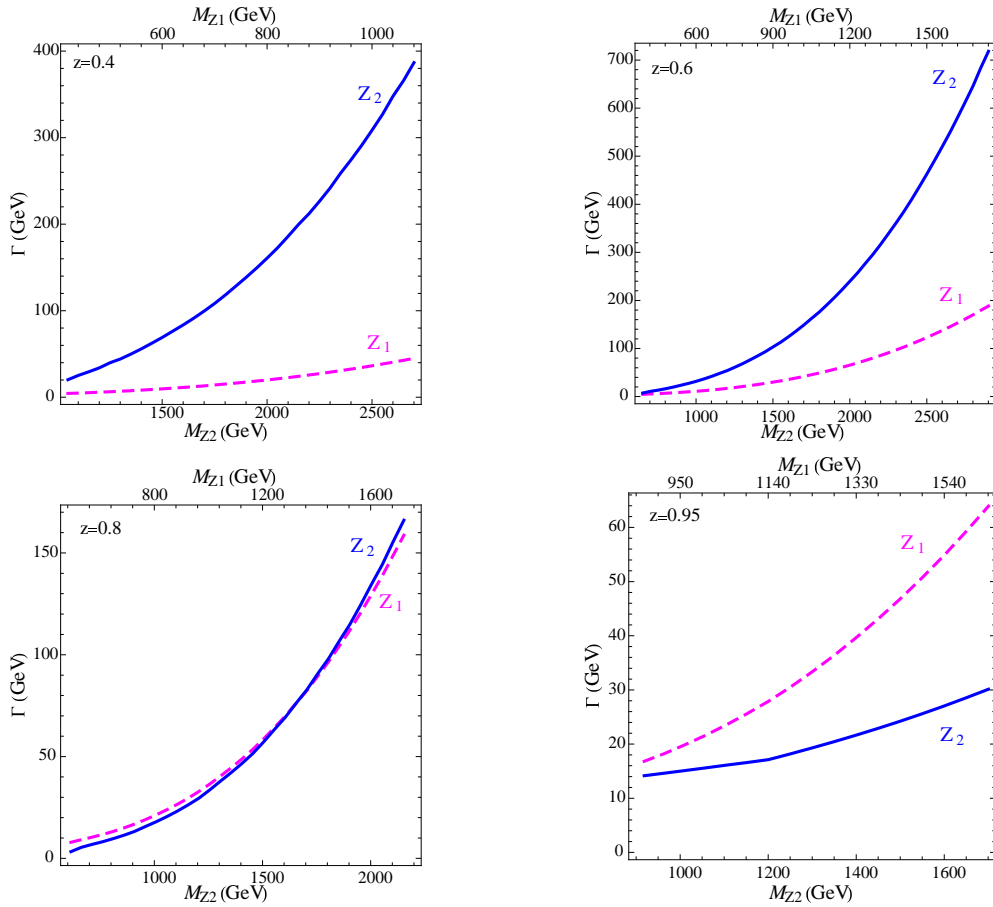


FIG. 3: Total decay width of Z_1 (magenta dashed line) and Z_2 (blue solid line) extra gauge bosons as a function of their mass, M_{Z_1} (upper x-axis) and M_{Z_2} (lower x-axis). The four plots refer to four different values of the free z -parameter: $z=0.4$ (top-left), $z=0.6$ (top-right), $z=0.8$ (bottom-left), $z=0.95$ (bottom-right).

R_{LHC} , while the green dot-dashed one refers to $0.5 \cdot \Gamma_{Z_1} = R_{LHC}$. In the righthand region of each curve, the corresponding total width could be measured. For comparison, we show also the same contour plots for the Tevatron assuming a mass resolution $R_{TEV} = 3.4\%M$ [39]. These are represented by the blue dashed and green dotted lines for the Z_2 and Z_1 bosons, respectively. As one can see, the Γ_{Z_1} -contour is almost independent on the Z_1 -boson coupling to fermions. The contour line simply shifts (very slightly) to higher mass values by increasing the z -parameter just because Γ_{Z_1} decreases correspondingly at fixed mass. The behaviour of the Γ_{Z_2} -contour is instead more complicated. It in fact depends on whether or not the decay into boson pairs is allowed. More the $Z_2 \rightarrow W_1 W$ phase space shrinks, more the decay into fermions becomes important. The contour lines acquire therefore a dependence on the Z_2 -boson coupling to ordinary matter, represented in the plot by the Z_2 -boson coupling to left-handed electrons \hat{a}_{2L}^e , which gets enhanced with the z -parameter.

Moreover, by increasing the z -parameter, the contour lines shift sensibly to higher mass values, as for the Z_1 -boson case. This trend continues until the $Z_{1,2}$ -boson widths get smaller than the mass resolution at both LHC and Tevatron in the full parameter space (i.e. all contour lines shift beyond the mass range allowed by the perturbative unitarity constraint). This is represented by the $z = 0.95$ scenario, which we do not explicitly display.

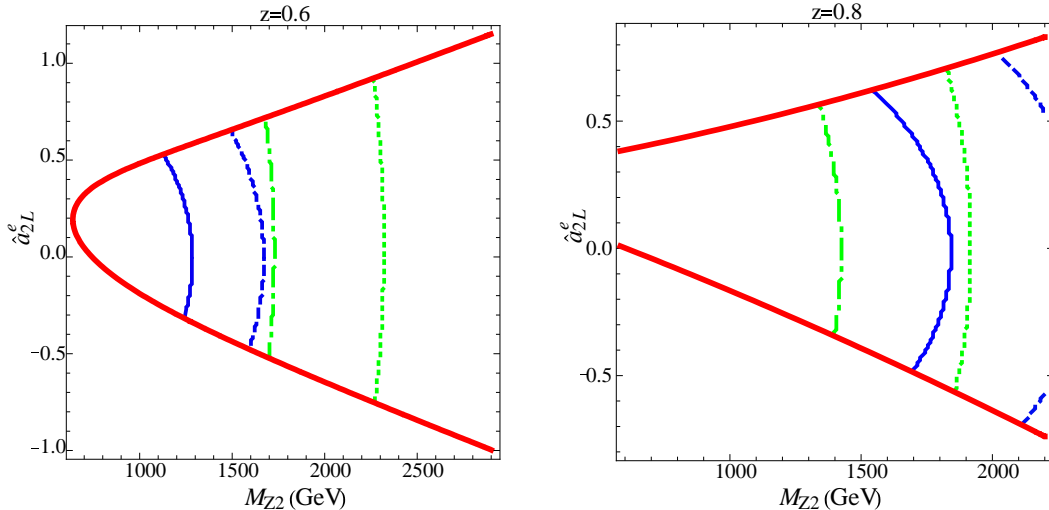


FIG. 4: Left: Contour plots in the plane $(M_{Z_2}, \hat{a}_{2L}^e)$ at fixed $z = 0.6$ representing the following requirements: $\Gamma_{Z_2}/2 = R_{LHC}$ (blue solid), $\Gamma_{Z_1}/2 = R_{LHC}$ (green dot-dashed), $\Gamma_{Z_2}/2 = R_{TEV}$ (blue dashed), and $\Gamma_{Z_1}/2 = R_{TEV}$ (green dotted) as explained in the text. Right: same as left-panel for $z = 0.8$. The total width can be measured in the righthand regions of the corresponding curve.

The possibility of measuring the width of the extra gauge bosons, at least in a sizeable part of the parameter space, is a distinctive feature of the four-site model. Common extra $U(1)$ theories present in the literature predict indeed an additional Z' -boson purely decaying into fermion pairs. As a consequence, the Z' width is generally expected to be very narrow and below the foreseen mass resolution at the LHC.

The $Z_{1,2}$ branching ratios are shown in Fig. 5 for three values of the z -parameter: $z=0.6, 0.8, 0.95$. Here we do not show the $z=0.4$ case as it does not differ sensibly from the $z=0.6$ scenario. The $Z_{1,2}$ -boson BRs into fermion pairs are evaluated by considering, for each mass value, the maximum coupling allowed by EWPT bounds. Let us discuss first the Z_1 branching ratios displayed on the leftside plots. The lighter extra gauge boson can decay into fermions and dibosons: $Z_1 \rightarrow f\bar{f}$ and $Z_1 \rightarrow WW$. In the figure, the branching in down-quarks, up-quarks, neutrinos (summed up over all generations), electrons and W-boson pairs

is shown. For all z -values, the diboson channel is the dominant one. The decay into electrons is below 2% (slightly increasing with the z -parameter), but it is anyhow competing if one relies on clean purely leptonic final states as $BR(Z_1 \rightarrow WW \rightarrow ee\nu_e\nu_e) = BR(Z_1 \rightarrow WW)/81$.

The Z_2 branching ratios are displayed on the right. The heavier extra gauge boson is purely axial up to electroweak corrections, hence it can decay into fermions and mixed diboson pairs: $Z_2 \rightarrow f\bar{f}$ and $Z_2 \rightarrow W_1W$ ($Z_2 \rightarrow WW$ and $Z_2 \rightarrow W_1W_1$ are highly suppressed). Once more, the competing coupling and phase space effects play a delicate role. Even if the decay into electron-pairs is always below 4%, the global branching ratio into fermions can become dominant. By increasing the z -parameter, the phase space for the mixed diboson decay gets reduced or even disappears, and the fermions take over as shown clearly in the bottom-right plot ($z=0.95$).

IV. DRELL-YAN PRODUCTION AT THE LHC AND THE TEVATRON

We can now consider the production of the two neutral gauge bosons, $Z_{1,2}$, predicted by the four-site Higgsless model at the LHC and the Tevatron through the Drell-Yan channel. Owing to the introduction of direct couplings between ordinary matter and extra gauge bosons, in addition to the usual indirect ones due to the mixing, the experimental bounds from electroweak precision data on the model parameters are indeed less stringent. As a consequence, and in contrast with the existing fermiophobic Higgsless literature, quite large couplings between SM fermions and extra gauge bosons are allowed (see Fig. 2).

A. Processes and their computation

We analyze in detail the neutral Drell-Yan channels

$$pp \rightarrow e^+e^-, \quad p\bar{p} \rightarrow e^+e^- \quad (19)$$

at the LHC and the Tevatron, respectively. The two channels differ only by the initial state, and are characterized by an isolated electron and positron in the final state. These processes can involve the production of the two additional gauge bosons, Z_1 and Z_2 , as intermediate states. They are described by the generic formula

$$d\sigma^{h_1h_2}(P_1, P_2, p_f) = \sum_{i,j} \int dx_1 dx_2 f_{i,h_1}(x_1, Q^2) f_{j,h_2}(x_2, Q^2) d\hat{\sigma}^{ij}(x_1 P_1, x_2 P_2, p_f), \quad (20)$$

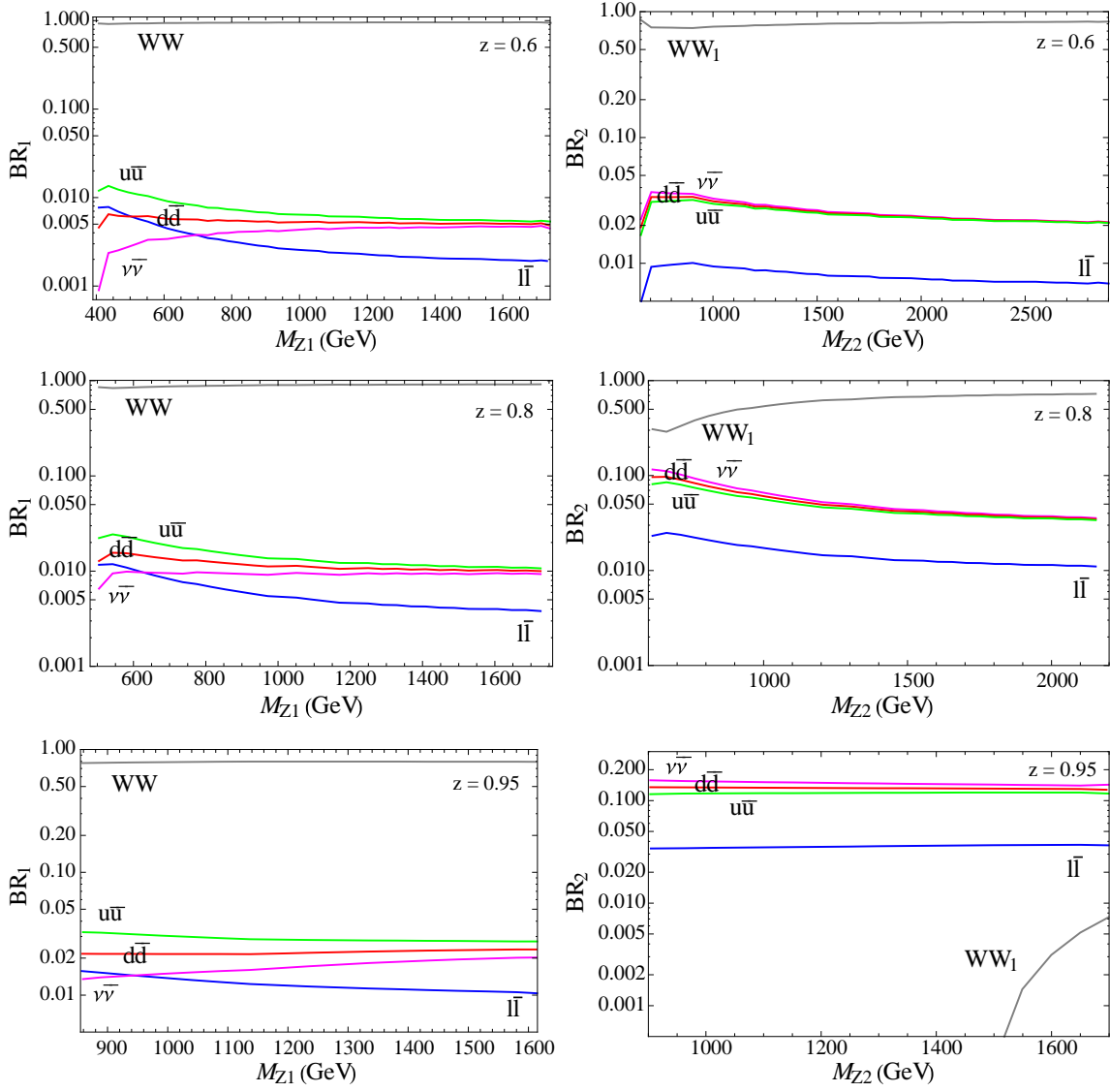


FIG. 5: Left: Z_1 -boson branching ratios as a function of its mass. Right: Z_2 -boson branching ratios versus its mass. From top to bottom, the free z -parameter assumes the three representative values: $z = 0.6, 0.8, 0.95$.

where p_f summarizes the final-state momenta, f_{i,h_1} and f_{j,h_2} are the distribution functions of the partons i and j in the incoming hadrons h_1 and h_2 with momenta P_1 and P_2 , respectively, Q is the factorization scale, and $\hat{\sigma}^{ij}$ represent the cross sections for the partonic processes. At the LHC, since the two incoming hadrons are protons and we sum over final states with

opposite charges, we find

$$d\sigma^{h_1 h_2}(P_1, P_2, p_f) = \int dx_1 dx_2 \sum_{Q=u,c,d,s,b} \left[f_{\bar{Q},p}(x_1, Q^2) f_{Q,p}(x_2, Q^2) d\hat{\sigma}^{\bar{Q}Q}(x_1 P_1, x_2 P_2, p_f) + f_{Q,p}(x_1, Q^2) f_{\bar{Q},p}(x_2, Q^2) d\hat{\sigma}^{Q\bar{Q}}(x_1 P_1, x_2 P_2, p_f) \right]. \quad (21)$$

At the Tevatron, since the two incoming hadrons are proton and anti-proton, the same observable reads instead as

$$d\sigma^{h_1 h_2}(P_1, P_2, p_f) = \int dx_1 dx_2 \sum_{Q=u,c,d,s,b} \left[f_{\bar{Q},p}(x_1, Q^2) f_{Q,\bar{p}}(x_2, Q^2) d\hat{\sigma}^{\bar{Q}Q}(x_1 P_1, x_2 P_2, p_f) + f_{Q,p}(x_1, Q^2) f_{\bar{Q},\bar{p}}(x_2, Q^2) d\hat{\sigma}^{Q\bar{Q}}(x_1 P_1, x_2 P_2, p_f) \right]. \quad (22)$$

The tree-level amplitudes for the partonic processes have been generated by means of PHACT [42], a set of routines based on the helicity-amplitude formalism of Ref. [43]. The matrix elements have been inserted in the Monte Carlo event generator FAST_2f, dedicated to Drell-Yan processes at the EW and QCD leading order. FAST_2f can compute simultaneously the new-physics signal and the SM background. It can generate cross-sections and distributions for any observable, including any kind of kinematical cuts. The code is moreover interfaced with PYTHIA [44]. This feature can allow a more realistic analysis, once FAST_2f is matched with detector simulation programs.

B. Numerical setup

For the numerical results presented here, we have used the following input values [45]: $M_Z = 91.187 \text{ GeV}$, $\Gamma_Z = 2.512 \text{ GeV}$, $\Gamma_W = 2.105 \text{ GeV}$, $\alpha(M_Z) = 1/128.88$, $G_F = 1.166 \times 10^{-5} \text{ GeV}^{-2}$. In our scheme, the weak mixing-angle and the W -boson mass are derived quantities. We use the fixed-width scheme for the matrix element evaluation, and the CTEQ6L[46] for the parton distribution functions at the factorization scale:

$$Q^2 = M_{\text{inv}}^2(e^+e^-) \quad (23)$$

where M_{inv} denotes the invariant mass. This scale choice appears to be appropriate for the calculation of differential cross sections, in particular for lepton distributions at high energy scales.

When considering the DY-channel at the LHC, we have moreover implemented a general set of acceptance cuts appropriate for LHC analyses, and defined as follows:

- lepton transverse momentum $P_T(l) > 20 \text{ GeV}$,
- lepton pseudo-rapidity $|\eta_l| < 2.5$, where $\eta_l = -\log(\tan \theta_l/2)$, and θ_l is the polar angle of the charged lepton l with respect to the beam.

For the process at hand, we have also used further cuts which are described in due time. We assume as electron detection efficiency $\epsilon_e = 90\%$ [40] and we present results for the 7 TeV LHC with an integrated luminosity $L = 1 \text{ fb}^{-1}$ and for the 14 TeV LHC with an integrated luminosity $L = 10 \text{ fb}^{-1}$.

For the study of the Drell-Yan channel at the Tevatron, we assume instead an overall signal acceptance of the order of 20% [47]. Moreover, we consider two values for the integrated luminosity: $L = 3.6 \text{ fb}^{-1}$ (recent preliminary D0 analysis) and $L = 10 \text{ fb}^{-1}$ (next two year projection).

C. $Z_{1,2}$ -boson production at the LHC and the Tevatron

The additional gauge bosons, predicted by the four-site Higgsless model, can be produced at the LHC via the DY process $pp \rightarrow \gamma, Z, Z_{1,2} \rightarrow e^+e^-$.

The corresponding total cross-sections, in the gauge boson mass interval allowed by unitarity bounds, are shown in Fig. 6 for three representative values of the free z -parameter: $z=0.6, 0.8, 0.95$. These are just bare values, useful only to give an idea of the magnitude of the expected cross-sections under the resonances. The displayed cross-sections have been in fact computed within the symmetric mass window,

$$|M_{\text{inv}}(e^+e^-) - M_{Z_1, Z_2}| \leq \max(\Gamma_{Z_1, Z_2}/2, R) \quad (24)$$

with R the estimated mass resolution for LHC and Tevatron. Moreover, they have been calculated for the maximum value of the Z_2 -boson coupling to left-handed electrons allowed by the EWPT for the given z -parameter.

The left-side panel of Fig. 6 shows the total cross-section under the Z_1 -resonance. The right-side panel refers to the Z_2 -boson. For each z value we plot the cross section, corresponding to the maximum coupling \hat{a}_{2L}^e allowed by EWPT, for $\sqrt{s} = 7$ and 14 TeV. At fixed mass, M_{Z_1, Z_2} , the $Z_{1,2}$ -boson cross-sections get larger by increasing the value of the z -parameter. This effect is due to the fact that high z -values help in relaxing EWPT con-

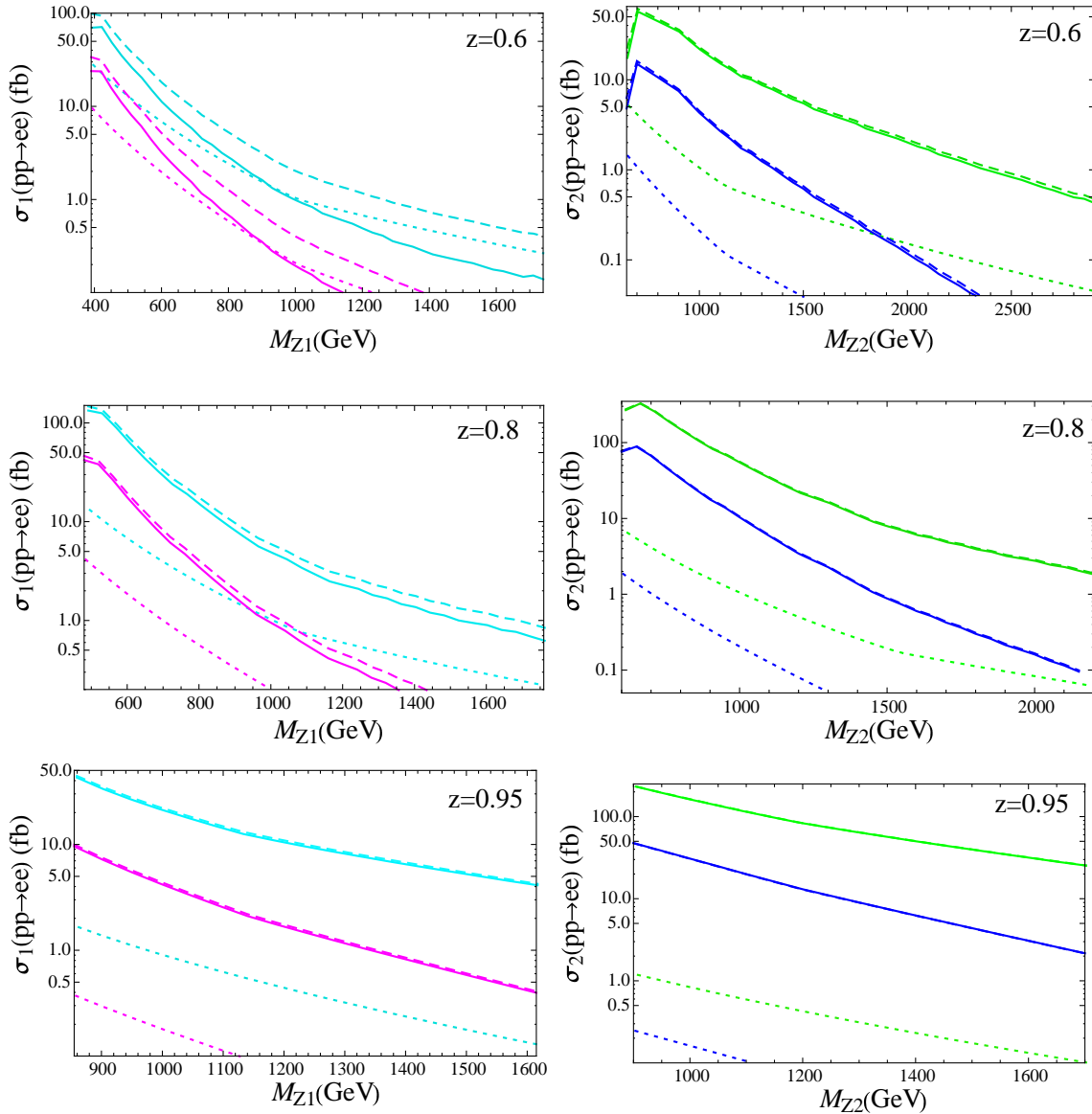


FIG. 6: Left: Z_1 -boson cross-sections for the maximal \hat{a}_{2L}^e allowed by EWPT, in the mass window given in Eq.(24), as a function of M_{Z_1} at the 7 TeV LHC (lower curves) and the 14 TeV LHC (upper curves). The dashed lines represent the total cross-sections (T), including the interference of the Z_1 -boson signal with both the SM background and the Z_2 -boson signal. The dotted lines show the SM backgrounds (B). The solid lines correspond to their differences: $S=T-B$. Right: same for the Z_2 -boson. From top to bottom, the free z -parameter assumes the three representative values: $z=0.6, 0.8, 0.95$.

straints on the $Z_{1,2}$ -boson coupling to SM fermions, as can be seen in Fig. 2 which shows the EWPT bounds on the representative Z_2 -boson coupling to electrons, \hat{a}_{2L}^e .

Moreover, while the total cross-section under the Z_1 -resonance is at most $\sigma_1 \simeq 50$ fb at

the 7 TeV LHC, the Z_2 -boson cross-section can be sensibly higher, of the order of $\sigma_2 \simeq 100$ fb. This is a consequence of an intrinsic property of the model. That is, in most part of the parameter space, the axial spin-one Z_2 -boson is more strongly coupled to fermions than the vector spin-one Z_1 -boson. This peculiarity is shown in Fig. 7 for two sample values of the free z -parameter: $z=0.6, 0.8$. This characteristic will have direct influence on the resonant

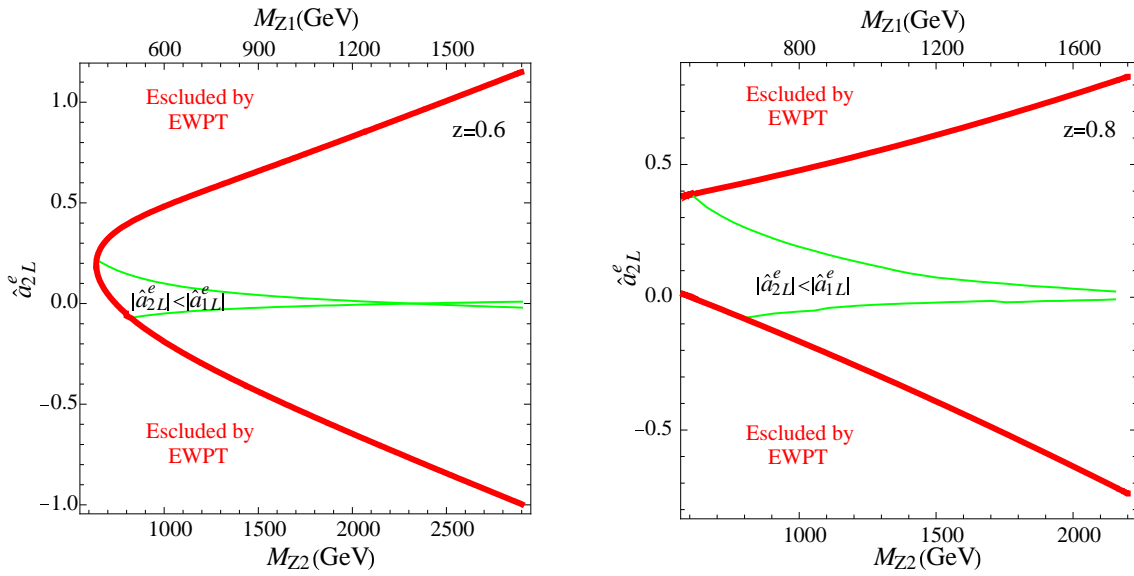


FIG. 7: The red thick solid line gives the parameter space allowed by EWPT. The green solid lines delimit the region where the Z_2 -boson coupling to electrons (\hat{a}_{2L}^e) is smaller than the Z_1 -boson coupling to electrons (\hat{a}_{1L}^e). We consider two sample values of the free z -parameter: $z=0.6$ (left-panel) and $z=0.8$ (right-panel).

peaking structure of the differential cross section, as we will see in the next section.

As comparison, we consider also the $Z_{1,2}$ -boson production at the Tevatron via the process $p\bar{p} \rightarrow \gamma, Z, Z_{1,2} \rightarrow e^+e^-$. In Fig. 8, we show the total cross-section under the $Z_{1,2}$ resonances as a function of the gauge boson masses, in perfect analogy with the LHC plots presented before. At the Tevatron, the expected cross section is always below 15 fb.

In order to estimate the LHC reach, we now consider in Table I different choices of mass spectrum. These examples give an idea of the possible scenarios predicted by the four-site Higgsless model. In the model in fact, as already mentioned, the ratio between the gauge boson masses of the first and second triplet, z , is a free parameter. Hence, the distance between the two masses is arbitrary as well. We have thus chosen three cases: $z = 0.6$ representing the flat-metric scenario (see [30]), giving rise to very distant resonances, $z = 0.8$

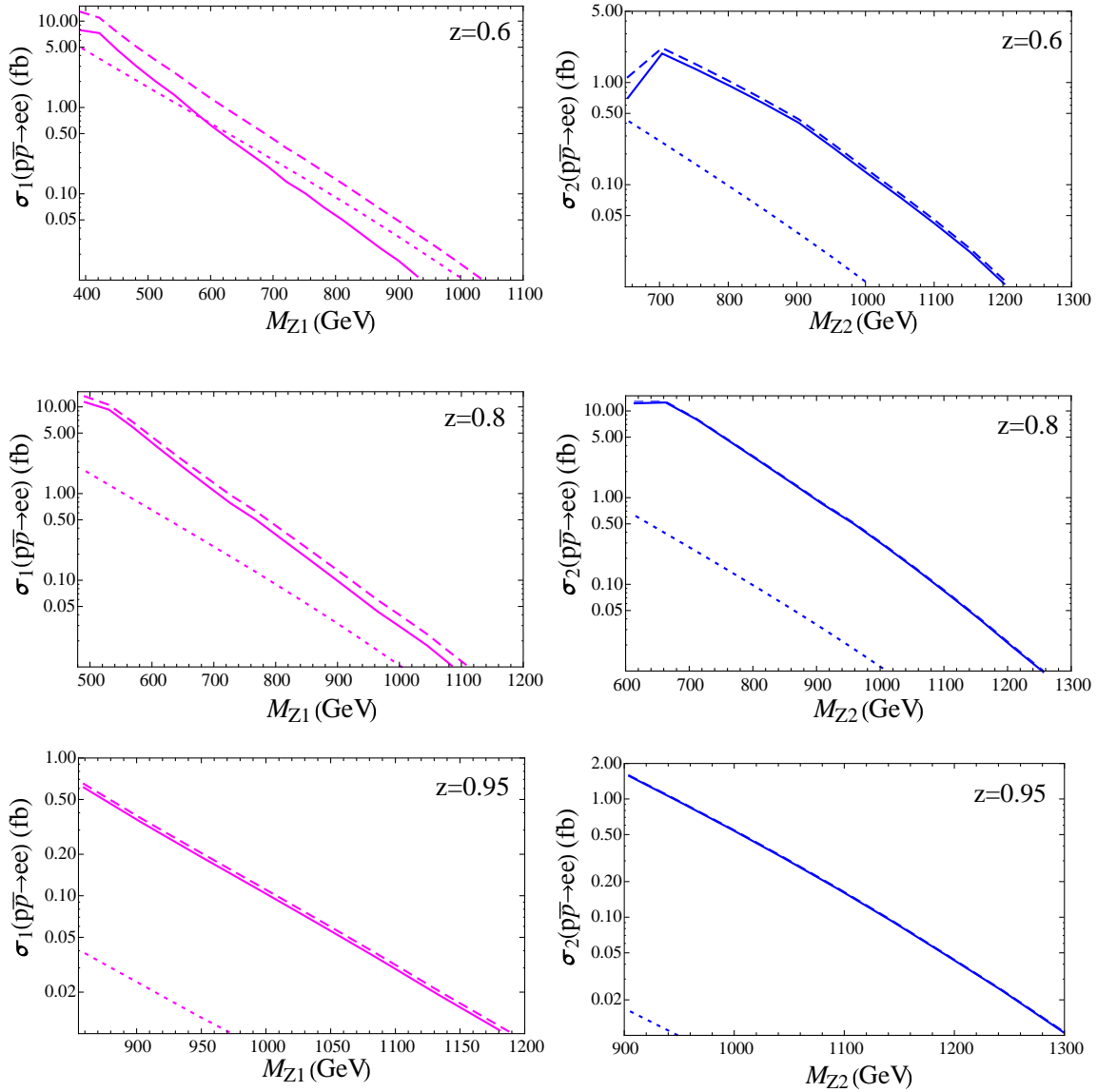


FIG. 8: Left: Z_1 -boson cross-sections, for the maximal \hat{a}_{2L}^e allowed by EWPT, in the mass window given in Eq.(24), as a function of M_{Z_1} at the Tevatron. The dashed line represents the total cross-section (T), including the interference of the Z_1 -boson signal with both the SM background and the Z_2 -boson signal. The dotted line shows the SM background (B). The solid line corresponds to their difference: $S=T-B$. Right: same for the Z_2 -boson. From top to bottom, the free z -parameter assumes the three representative values: $z = 0.6, 0.8, 0.95$.

which is a case where the $Z_{1,2}$ bosons are closer in mass but still separately measurable, and finally $z = 0.95$ corresponding to a spectrum which tends to degeneracy by approaching the limit $z \rightarrow 1$.

For each z -value, we then consider two sets of $M_{Z_{1,2}}$ masses. The first one corresponds

$z = 0.6$	M_{Z_1, Z_2} (GeV)	Γ_{Z_1, Z_2} (GeV)	\hat{a}_{2L}^e	\hat{a}_{1L}^e
a	436, 704	5.4, 10.8	0.33	0.23
b	552, 903	8.8, 23.7	0.45	0.23

$z = 0.8$	M_{Z_1, Z_2} (GeV)	Γ_{Z_1, Z_2} (GeV)	\hat{a}_{2L}^e	\hat{a}_{1L}^e
c	505, 614	7.9, 3.3	0.29	0.33
d	893, 1107	26.6, 23.3	0.50	0.36

$z = 0.95$	M_{Z_1, Z_2} (GeV)	Γ_{Z_1, Z_2} (GeV)	\hat{a}_{2L}^e	\hat{a}_{1L}^e
e	889, 968	16.8, 14.2	0.60	0.45
f	1359, 1433	39.6, 21.6	0.64	0.49

TABLE I: Six representative scenarios for the four-site Higgsless model. In the tables, M_{Z_1, Z_2} and Γ_{Z_1, Z_2} are physical masses and widths of the $Z_{1,2}$ -bosons, and \hat{a}_{1L}^e , \hat{a}_{2L}^e represent the $Z_{1,2}$ -boson couplings to the left-handed electron.

to the point in the parameter space, allowed by EWPT and by direct Tevatron limits (see next section), which ensures the maximal cross-section. And, typically, it coincides with the minimum allowed mass. The latter set refers instead to the case in which one reaches the 5-event threshold in order to claim a discovery at the LHC with $\sqrt{s} = 7$ TeV and $L = 1$ fb $^{-1}$. We always assume to work with the maximum value of the Z_2 -boson coupling to SM fermions for any given mass and z -value. This means that we move along the upper part of the contour plots which delimit the area allowed by EWPT in the plane $(M_{Z_2}, \hat{a}_{2L}^e)$, shown in Fig. 2.

We are now ready to present some differential cross sections for the leptonic process $pp(p\bar{p}) \rightarrow e^+e^-$. As an illustration of the behaviour and the impact of the new predicted particles at the LHC, in the following we analyze the distribution in the invariant mass of the reconstructed $Z_{1,2}$ -boson, that is $M_{\text{inv}}(e^+e^-)$. In the previous section, we have seen that there is a lower bound on the $Z_{1,2}$ -boson masses: $M_{Z_1} > 350$ GeV and $M_{Z_2} > 500$ GeV. We thus select this energy scale by imposing an additional cut on the invariant mass of the lepton pair, i.e. $M_{\text{inv}}(e^+e^-) \geq 200$ GeV. In Fig. 9, we plot the total number of events divided by a 10 GeV bin as a function of the dilepton invariant mass for the six aforementioned scenarios. We have checked that all these cases are outside the exclusion limit from direct searches at the Tevatron with an integrated luminosity $L = 3.6$ fb $^{-1}$ [47] (see next section).

These examples show four peculiarities of the model. First of all, the masses of the two neutral resonances $Z_{1,2}$ are not equally spaced. They can be either very distant for

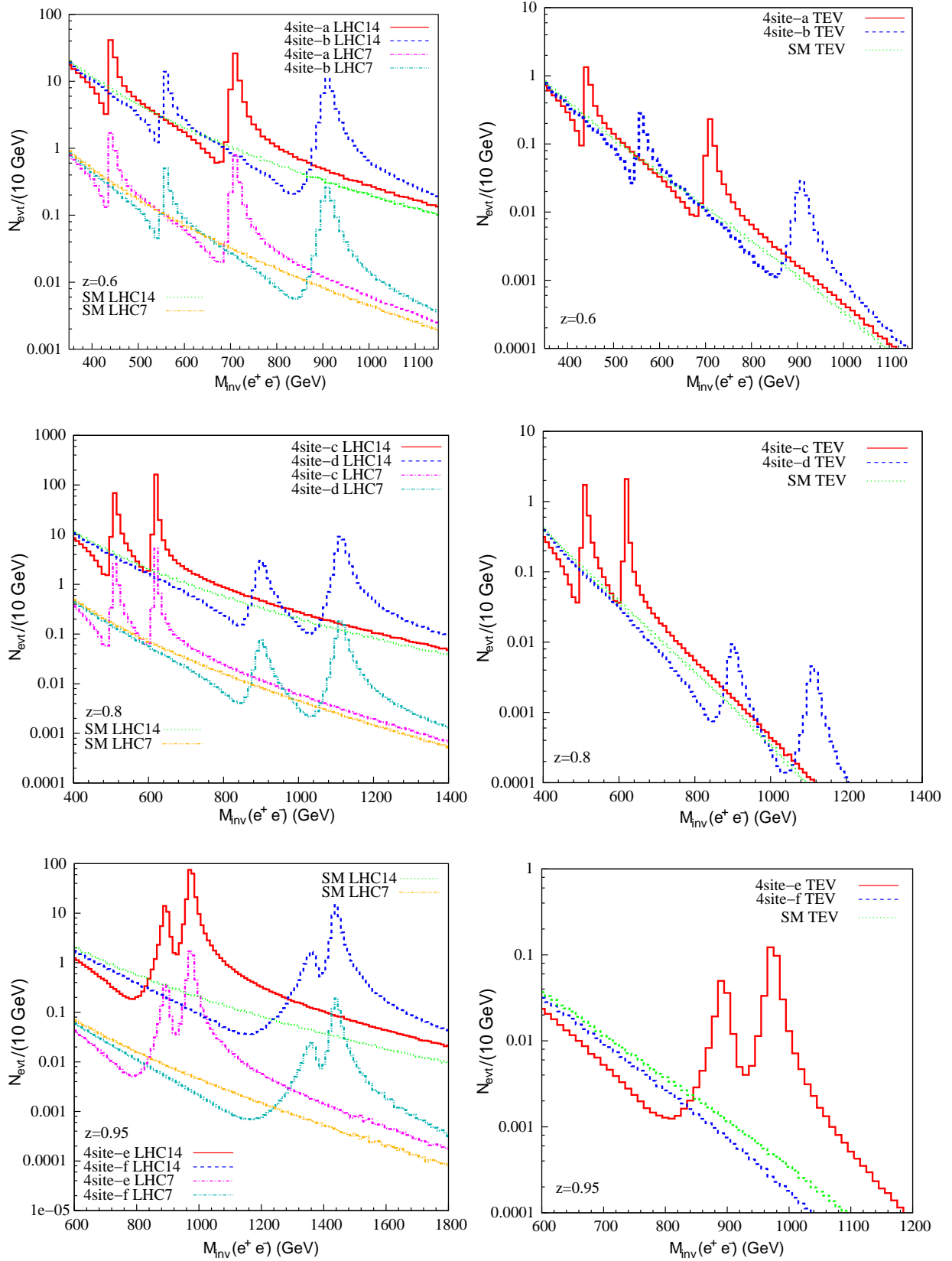


FIG. 9: Left: Total number of events over a 10 GeV-bin versus the dilepton invariant mass, $M_{\text{inv}}(e^+e^-)$, for the process $pp \rightarrow e^+e^-$ at the 7 TeV LHC with $L=1 \text{ fb}^{-1}$ (lower curves) and at the 14 TeV LHC with $L=10 \text{ fb}^{-1}$ (upper curves), for the scenarios given in Table I. From top to bottom: $z=0.6$, 0.8, and 0.95. Standard cuts and a 90% detection efficiency for the electron is included. Right: same as in the left panel for the process $p\bar{p} \rightarrow e^+e^-$ at the 1.96 TeV Tevatron

low z -values (see top-left panel in Fig. 9), or they can tend to be almost degenerate for high z -values (see bottom-left panel in Fig. 9). For some values of the parameter space (see for example the b , d and f scenarios), one of the two resonances could also disappear leaving a single-resonant spectrum. In this case, the distinctive multi-resonant peaking structure of the four-site model would be hidden, making the Higgsless model to become highly degenerate with common extra U(1) theories predicting just one additional Z' -boson. The same situation would happen for $z = 0.95$ (see bottom-left panel in Fig. 9), if the mass resolution were not small enough to allow a separate measurement of the two resonances.

A second feature is related to the interference between signal and SM background. All plots exhibit indeed a sizeable depletion of the total number of events, compared to the SM prediction, in the off-peak region. A further distinctive behaviour is represented by the width magnitude. It indeed increases with the third power of the extra gauge boson mass. One can thus pass from configurations with very narrow resonances to scenarios characterized by broad peaks (or even shoulders). The last feature concerns the relative size of the $Z_{1,2}$ resonances. In Fig. 7, we have indeed shown that in most part of the parameter space the Z_1 -fermion couplings are smaller than the Z_2 -fermion ones. As a consequence, the height of the Z_1 -resonance is less pronounced than the Z_2 -peak. This feature can be washed out by the PDF effect, but it is clearly visible in Fig. 9.

In order to compare the LHC reach at $L = 1 \text{ fb}^{-1}$ with the discovery potential of the Tevatron projected at $L = 10 \text{ fb}^{-1}$, in Fig. 9 (right panel), we plot the $Z_{1,2}$ spectrum for the same setups (only the first setup of the $z=0.95$ scenario is shown in the bottom-right panel). We display the total number of events over a 10 GeV bin expected for the two colliders.

To have an idea of the detection rate expected at the LHC with $\sqrt{s} = 7 \text{ TeV}$ and $L=1 \text{ fb}^{-1}$ for the Drell-Yan production of the extra $Z_{1,2}$ gauge bosons, in Tab. II we have listed signal and background event number in the two distinct on-peak regions $|M_{\text{inv}}(e^+e^-) - M_{Z_1, Z_2}| < \max(\Gamma_{Z_1, Z_2}/2, R_{LHC})$ for the six considered scenarios. The signal event number is calculated as the difference between the total number of events and the background. The Tevatron expected rates for the same six setups, calculated for 10 fb^{-1} with the same procedure, turn out to be much smaller and only the case c gives sizeable statistical significance ($\sigma(Z_1) = 11.7$ and $\sigma(Z_2) = 26.0$).

	M_{Z_1, Z_2} (GeV)	$\Gamma_{1,2}$ (GeV)	$N_{\text{evt}}^{\text{sig}}(Z_1)$	$N_{\text{evt}}^{\text{backg}}(Z_1)$	$\sigma(Z_1)$	$N_{\text{evt}}^{\text{sig}}(Z_2)$	$N_{\text{evt}}^{\text{backg}}(Z_2)$	$\sigma(Z_2)$
a	436,704	5.4,10.8	17	5	7.6	12	1	12.0
b	552,903	8.8,23.7	5	2	3.5	6	1	6.0
c	505,614	7.9,3.3	31	3	17.9	59	1	59.0
d	893,1107	26.6,23.3	1	1	1.0	5	1	5.0
e	889,968	16.8,14.2	8	1	8.0	39	1	39.0
f	1359,1433	39.6,21.6	1	1	1.0	5	1	5.0

TABLE II: The first three columns represent the scenario. The next three columns give signal (including the interference with the SM background) and SM background event number for the Z_1 production, and the statistical significance $\sigma = N_{\text{evt}}^{\text{sig}}/\sqrt{N_{\text{evt}}^{\text{backg}}}$ at the LHC with $\sqrt{s} = 7$ TeV and $L=1 \text{ fb}^{-1}$. The last three columns show the same results for the Z_2 production.

V. $Z_{1,2}$ EXCLUSION AND DISCOVERY REACH AT THE TEVATRON AND THE LHC

In this section, we discuss the prospects of discovering the two neutral spin-1 bosons predicted by the four-site Higgsless model at the Tevatron and LHC.

Let us start by deriving the present exclusion limits on $Z_{1,2}$ -bosons from the Tevatron experiment. We take as a reference the recent preliminary analysis of the neutral DY-channel into electron-pairs performed by the D0 collaboration at the collected luminosity $L=3.6 \text{ fb}^{-1}$ [47]. There, observed and expected 95% C.L. upper limits on $\sigma(\text{p}\bar{\text{p}} \rightarrow Z') \times Br(Z' \rightarrow ee)$ are derived as a function of $M_{Z'}$. More in detail, the D0 95% C.L. sensitivity to an hypothetical Z' -boson has been derived by calculating the DY cross section upper bound within an asymmetric mass window around the x-axis M-value, i.e. $M_{\text{inv}}(e^+e^-) \geq M - 3R_{TEV}$ where $R_{TEV} \simeq 3.4\%M$ is the approximated D0 mass resolution (see Ref. [47] and references therein). A global signal acceptance of about 20% is included (its precise value depends on the energy scale as described in Ref. [47]). This allows one to extract direct limits on the Z' -mass from the purely deconvoluted, uncut, theoretical DY cross section within any given extra $U(1)$ model.

Following the D0 *strategy*, the limit on the four-site model has been obtained by computing the DY cross section in the interval $M_{\text{inv}}(e^+e^-) \geq M_{Z_1} - 3R_{TEV}$, in order to include the

effect of both $Z_{1,2}$ resonances, and assuming for each M_{Z_1} -mass the maximal \hat{a}_{2L}^e -coupling allowed by EWPT. No cuts and no detection efficiency are included. The mass limit on the lightest Z_1 -boson is extracted from the intersection of the theoretical cross section and the 95% C.L. upper bound derived from the observed data. The four-site model is much less constrained compared to other popular Z' theories owing to generally smaller couplings between SM fermions and extra gauge bosons. Assuming maximal values for the $Z_{1,2}$ -boson couplings to SM fermions, the direct mass limit is in fact given by: $M_{Z_1} \geq 520 \text{ GeV}$ for $z=0.8$. For smaller z -values, EWPT give very strong bounds on \hat{a}_{2L}^e in the low mass region so that Tevatron is not effective. For higher z -values, the mass range allowed by the x -approximation is out of the present Tevatron reach.

Starting from the above-mentioned limit on the $Z_{1,2}$ -boson mass at fixed z -value, we have extended the D0 exclusion criteria to the full parameter space allowed by EWPT for the three reference choices of the z parameter: $z = 0.6, 0.8$ and 0.95 . The result is represented by an excluded region in the conventional plane $(M_{Z_2}, \hat{a}_{2L}^e)$. In Fig. 10, for $z = 0.8$ the portion of the parameter space excluded by the present D0 data is depicted as a black triangle area (for the other choices of the z parameter the present Tevatron data give no restrictions).

As a useful statistical tool, we have moreover verified that the exclusion contour in the plane $(M_{Z_2}, \hat{a}_{2L}^e)$ at fixed z -value that is obtained by intersecting the theoretical cross section with the 95% C.L. upper bound coming from the expected SM background coincides, with good accuracy, with the exclusion contour derived by using the Poisson statistical indicator [48]. The agreement is within a few per mill once the D0 signal acceptance is included in the evaluation of the Poisson distribution. When discussing future prospects of discovering or excluding the four-site Higgsless model at Tevatron and LHC, we will thus rely on the Poisson statistics.

In the following, we compare the $Z_{1,2}$ -boson exclusion and discovery reach at the upgraded Tevatron with luminosity $L=10 \text{ fb}^{-1}$, and at the 7 TeV LHC with $L=1 \text{ fb}^{-1}$. We assume the signal acceptance setups described in Sec. IV B.

In the left panel of Fig. 10, we show the exclusion contour plots in the plane $(M_{Z_2}, \hat{a}_{2L}^e)$ for three values of the free z -parameter: $z=0.6, 0.8, 0.95$ from top to bottom. The black triangle represents the exclusion region based on recent preliminary D0 data, as explained above. The solid blue line indicates the 2σ -exclusion potential that Tevatron should reach in the next two years, i.e. assuming a project luminosity $L=10 \text{ fb}^{-1}$. Finally, the dot-dashed

green line gives the 2σ -exclusion reach at the 7 TeV LHC, assuming an integrated luminosity $L=1 \text{ fb}^{-1}$. In absence of data, these contour plots have been computed by making use of the Poisson distribution, as mentioned above. They have been derived by applying the D0 counting strategy previously described, i.e. by integrating the cross section in the domain $M_{\text{inv}}(e^+e^-) \geq M_{Z_1} - 3R_{TEV}$, and taking into account the signal acceptance given in Sec. IV B. While in the next two years Tevatron could exclude the four-site model up to energy scales of the order of $M_{Z_2} \gtrsim 750, 880, 1050 \text{ GeV}$, for maximal \hat{a}_{2L}^e couplings allowed by EWPT and $z = 0.6, 0.8, 0.95$ respectively, the early stage of the LHC could extend this range to the mass limit $M_{Z_2} \gtrsim 950, 1400 \text{ GeV}$ for $z = 0.6, 0.8$ respectively and will cover the whole mass range allowed by the unitarity bound for $z = 0.95$.

In the right panel of Fig. 10, we show instead the discovery contour plot in the plane $(M_{Z_2}, \hat{a}_{2L}^e)$ for $z=0.6, 0.8, 0.95$ from top to bottom. As for the left panel, the black triangle represents the exclusion region based on recent preliminary D0 data. The procedure we apply in order to derive the discovery reach at the Tevatron and the LHC is different from the D0 counting strategy adopted for the exclusion contour plots. In this case, we aim in fact to distinguish the Z_1 and Z_2 -resonances. Hence, we pursue a shape reconstruction analysis. We thus calculate the cross section below each resonant peak, taking into account signal, SM background and their mutual interference. Following Ref. [39], we select the mass window $|M_{\text{inv}}(e^+e^-) - M_{Z_{1,2}}| \leq \max(0.5 \times \Gamma_{Z_{1,2}}, R)$ where R is the mass resolution at Tevatron (R_{TEV}) or LHC (R_{LHC}), and we include the signal acceptance as given in Sec. IV B. By applying the Poisson statistical method, we obtain the $Z_{1,2}$ -boson discovery potential shown in the right panel of Fig. 10. The green dot-dashed (blue solid) line indicates the Z_1 (Z_2) discovery contour that Tevatron should be able to cover in the next two years, i.e. assuming a project luminosity $L = 10 \text{ fb}^{-1}$. As a comparison, the green dotted (blue dashed) line shows the Z_1 (Z_2) discovery reach at the 7 TeV LHC, assuming an integrated luminosity $L=1 \text{ fb}^{-1}$.

As one can see, independently on the collider, the Z_2 -boson discovery potential is enhanced compared to the Z_1 -boson. This is due to the nature of the two spin-1 particles in the four-site model, which has peculiar consequences on the structure of the $Z_{1,2}$ -boson couplings to the ordinary matter (see Fig. 7). Still, there are regions in the parameter space where the two resonances could be simultaneously observed. For example, for $z = 0.8$ up to energy scales of the order of $M_{Z_2} \simeq 700 (900) \text{ GeV}$ at the Tevatron (LHC), the four-site Hig-

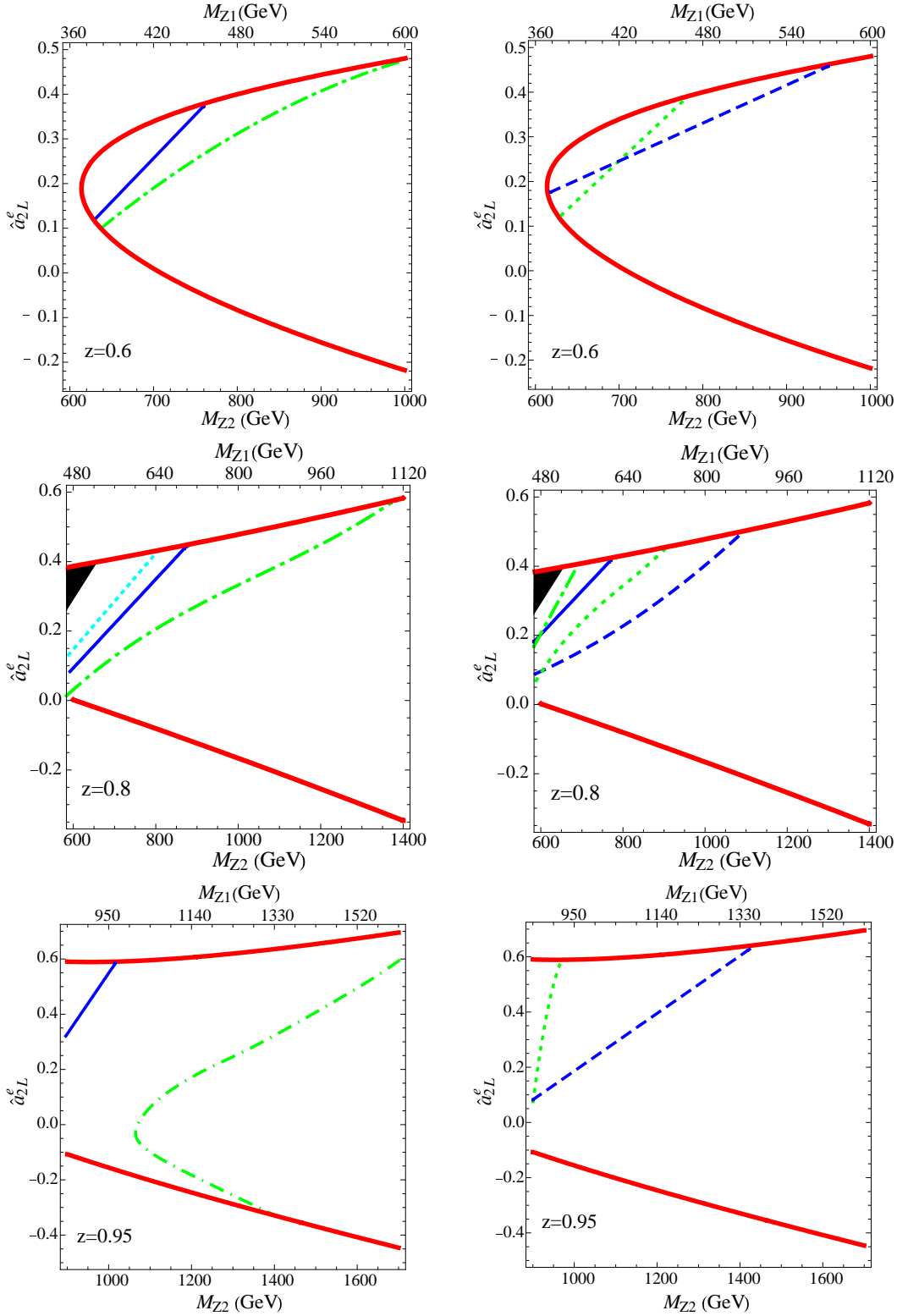


FIG. 10: Left: Exclusion at the Tevatron with $L=10 \text{ fb}^{-1}$ (solid blue line), and at the 7 TeV LHC with $L=1 \text{ fb}^{-1}$ (dot-dashed green line). The black triangle represents the exclusion limit from recent preliminary D0 data taken at $L=3.6 \text{ fb}^{-1}$. As comparison, the dashed cyan line shows the expected exclusion limit from the Tevatron with 3.6 fb^{-1} . Right: Z_1 -boson discovery (dot-dashed green line) and Z_2 -boson discovery (solid blue line) at the Tevatron with $L=10 \text{ fb}^{-1}$. Also shown, the Z_1 -boson discovery (green dotted line) and the Z_2 -boson discovery (blue dashed line) at the 7 TeV LHC with $L=1 \text{ fb}^{-1}$. From top to bottom: $z=0.6, 0.8, 0.95$. The thick red solid lines give

gless model could manifest its distinctive multi-resonance signature. Beyond those scales, only the Z_2 -boson could be visible giving rise to the well known degeneracy problem which affects all extra $U(1)$ theories. Leaving apart these problematics, which are beyond the scope of this paper, the global discovery reach during the early run of the LHC is substantial. The Z_2 -boson could be detected up to $M_{Z_2} \lesssim 950, 1100, 1400$ GeV at the 7 TeV LHC with $L = 1 \text{ fb}^{-1}$ for $z = 0.6, 0.8, 0.95$ respectively. Owing to the poor signal acceptance, the Tevatron with $L = 10 \text{ fb}^{-1}$ is not expected to go beyond $M_{Z_2} \leq 770$ GeV for $z = 0.8$ and it is not effective for $z = 0.6, 0.95$. Looking at the future, in Fig. 11 we show exclusion and discovery contours at the 14 TeV LHC with $L = 10 \text{ fb}^{-1}$. We consider the same signal acceptance as in Sec. IV B. We take as representative example the case $z = 0.8$ and we plot also a corresponding contours for the 7 TeV LHC for comparison. We see that the second stage of LHC could show the two resonance signature in the electron channel of the Drell-Yan process up to $M_{Z_2} = 2 \text{ TeV}$ (for $z = 0.8$). Notice that in our previous analysis [30] we did not include any reconstruction efficiency and we summed over electrons and muons. In this work we focused only on the electron channel, following the D0 data analysis on high mass neutral resonance search in Drell-Yan process. Similar limits are derived by the CDF collaboration using the muon channel. The two channels could be combined, in order to improve the statistics, taking into account the different efficiencies [39].

To conclude, for the same case $z = 0.8$, we show in Fig. 12 the minimum luminosity needed to claim a $Z_{1,2}$ -boson discovery during the early stage (left panel) and project stage (right panel) of the LHC. While the 7 TeV LHC would need very high luminosity ($L \simeq 200 \text{ fb}^{-1}$) to cover the entire mass range, its 14 TeV upgrade could give full discovery with only 15 fb^{-1} .

VI. CONCLUSIONS

In this paper, we have studied the phenomenology of the four-site Higgsless model, which is an extension of the minimal three-site version (BESS model). The four-site model is a deconstructed theory based on the $SU(2)_L \times SU(2)_1 \times SU(2)_2 \times U(1)_Y$ gauge symmetry. It predicts four charged ($W_{1,2}^\pm$) and two neutral ($Z_{1,2}$) extra gauge bosons. We have focused on the properties of the neutral gauge sector and on its discovery prospects at the Tevatron and the 7 TeV LHC in the dielectron channel during the next two years.

The phenomenology of the four-site model is controlled by only three free parameters

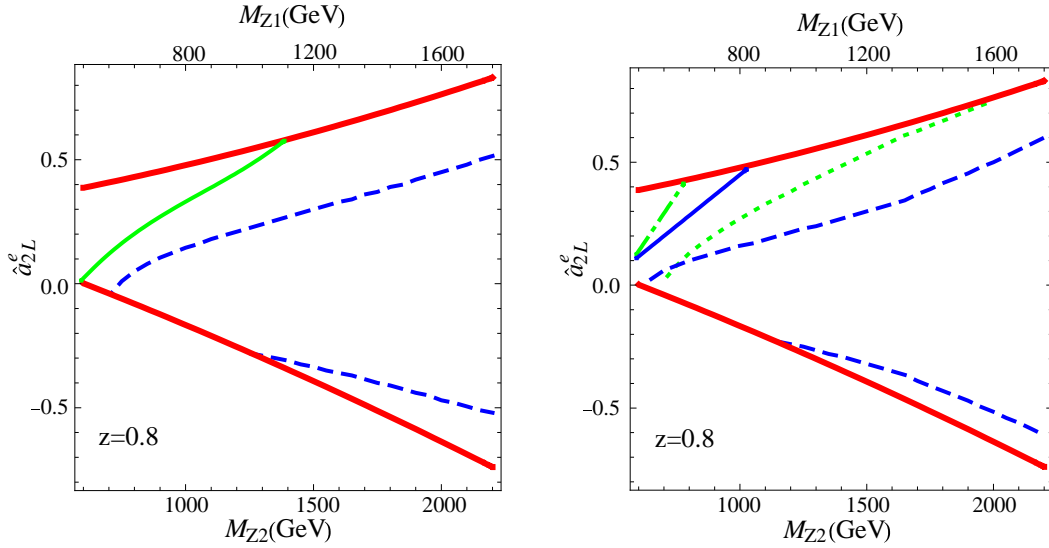


FIG. 11: Left: Exclusion at the 7 TeV LHC with $L=1 \text{ fb}^{-1}$ (solid green line), and at the 14 TeV LHC with $L=10 \text{ fb}^{-1}$ (dashed blue line). Right: Z_1 -boson discovery (dot-dashed green line) and Z_2 -boson discovery (solid blue line) at the 7 TeV LHC with $L=1 \text{ fb}^{-1}$. Also shown, as comparison, the Z_1 -boson discovery (green dotted line) and the Z_2 -boson discovery (blue dashed line) at the 14 TeV LHC with $L=10 \text{ fb}^{-1}$. All curves have been derived for $z=0.8$. The thick red solid lines give the allowed parameter space from EWPT.

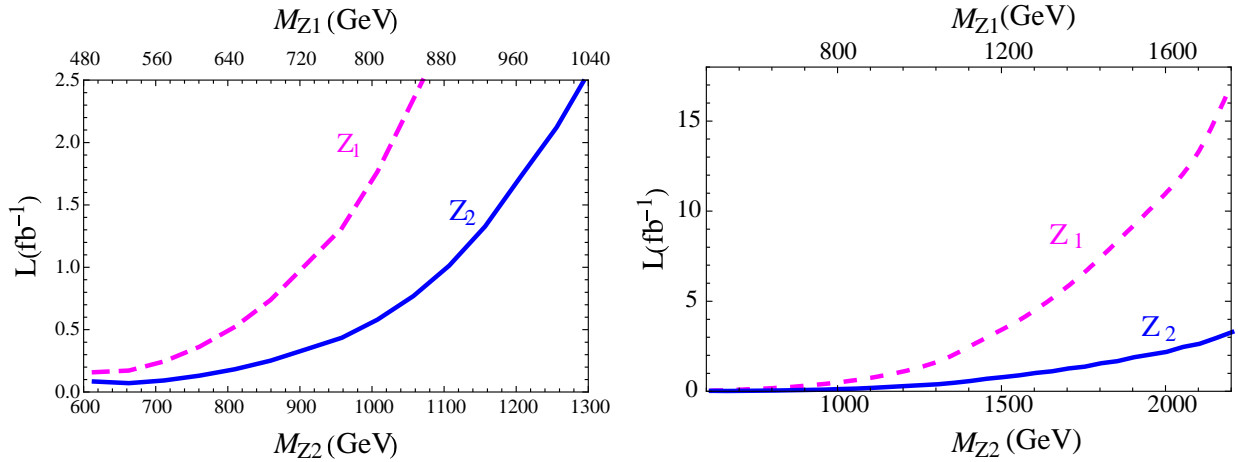


FIG. 12: Left: Minimum luminosity needed for a 5σ -discovery of Z_1 (dashed magenta line) and Z_2 (solid blue line) at the 7 TeV LHC, assuming maximal Z_2 -boson couplings to SM fermions and $z=0.8$. Right: same curves at the upgraded 14 TeV LHC.

beyond the SM ones: the two $Z_{1,2}$ -boson masses and the Z_2 -boson coupling to SM electrons. At fixed ratio $z = M_1/M_2 \simeq M_{Z_1}/M_{Z_2}$, the model can be thus visualized in the $(M_{Z_2}, \hat{a}_{2L}^e)$ plane. The parameter space has a twofold bound. On one side, unitarity requirement and $\mathcal{O}(x)$ -approximation restrict the calculability of the model within the following mass range: $350 \leq M_{Z_1} \leq 1800$ GeV and $600 \leq M_{Z_2} \leq 3000$ GeV. On the other side, EWPT constrain the \hat{a}_{2L}^e coupling. Nevertheless, the allowed parameter space is sizeable. This represents the major novelty of the four-site model which, in contrast to common Higgsless theories, can solve the dichotomy between unitarity and EWPT bounds without imposing the extra vector bosons to be fermiophobic. As a consequence, the Drell-Yan process becomes a relevant channel for the direct search of extra gauge bosons at the LHC and the Tevatron.

We have first described main properties and shape of the new $Z_{1,2}$ -bosons. We have shown their total widths and branching ratios into fermions and bosons. The results can be summarized in two points. First, even if $Z_{1,2}$ decay preferably into bosons, BRs into lepton pairs and boson pairs decaying in turn into leptons can compete, when looking at purely leptonic final states. For the four-site Higgsless model, the DY process is thus a strong discovery channel. Second, in contrast to common Z' -bosons which purely decay into SM fermions and appear as narrow resonances, $Z_{1,2}$ can display a broad peaking structure. Their total width could be measured in large portions of the parameter space, offering one more challenge to the experiments. In order to show what signature might be expected, we have presented three sample scenarios corresponding to different points in the parameter space. Here, the two $Z_{1,2}$ -bosons could appear as resonances either quite distant in mass or almost degenerate. If $M_{Z_1} \simeq M_{Z_2}$, two problems arise: their experimental separability or their collapse into just one peak. In this latter event, the four-site model would loose its characteristic multi-resonant structure becoming degenerate with common single- Z' models.

We have then computed the present direct limits on $Z_{1,2}$ -boson masses and coupling from recent searches performed by the D0 collaboration at the Tevatron with collected luminosity $L=3.6$ fb $^{-1}$. The outcome is that the four-site model is weakly bounded: only a small corner around the minimum mass, $M_{Z_2} \simeq 600$ GeV, has been excluded up to now.

The (almost) full parameter space is thus an open ground for the next two year experiments at the Tevatron and the LHC. Owing to low signal acceptance ($\simeq 20\%$) and reduced energy, the Tevatron with project luminosity $L=10$ fb $^{-1}$ is not expected to play a major role in the $Z_{1,2}$ -boson discovery. Its exclusion bounds can however extend up to 1 TeV scale.

These rates get enhanced at the 7 TeV LHC which by the end of 2011 should reach an integrated luminosity $L=1 \text{ fb}^{-1}$. Already in the next few months, with a preliminary luminosity of 50 pb^{-1} , the LHC can recover the present exclusion limits from Tevatron data. By collecting additional luminosity, the 7 TeV LHC should then be able to discover new physics predicted by the four-site Higgsless model up to 1400 GeV. The exclusion limits could cover the whole mass spectrum, depending on model parameters.

Finally, looking at the future, we have shown how the project 14 TeV LHC with $L=10 \text{ fb}^{-1}$ could sensibly extend the four-site physics search to regions of the parameter space with small $Z_{1,2}$ -boson couplings to ordinary matter.

Note added in proof. During completion of this work, we became aware of latest results obtained by the D0-collaboration on the search for a heavy neutral gauge boson in the dielectron channel at the Tevatron with 5.4 fb^{-1} , published in Ref.[49]. The new 95% C.L. upper limit on the Z' cross section can shift the $Z_{1,2}$ -boson mass bound up to $M_{Z_2} \simeq 800 \text{ GeV}$ in a small portion of the parameter space ($z=0.8$ and maximal \hat{a}_{2L}^e coupling). The projection for the next two year running at the Tevatron is basically unchanged.

Acknowledgments

LF would like to thank the School of Physics and Astronomy of the University of Southampton for hospitality. We are very grateful to L. Basso and G. M. Pruna for comparisons. We also acknowledge S. King, A. Belyaev and C. H. Shepherd-Themistocleous for valuable discussions.

Appendix A: Gauge boson trilinear couplings

The general form for the trilinear vertex is the following:

$$\mathcal{L}_3 = i \sum_{R,P,Q} a_{RPQ} (R_{\mu\nu}^+ P_\mu^- Q_\nu - P_{\mu\nu}^- R_\mu^+ Q_\nu + Q_{\mu\nu} P_\mu^+ R_\nu^-) \equiv i \sum_{R,P,Q} a_{RPQ} O_{RPQ} \quad (\text{A1})$$

where $R, P = W, W_1, W_2$ and $Q = \gamma, Z, Z_1, Z_2$ and

$$a_{WW\gamma} = a_{W_1W_1\gamma} = a_{W_2W_2\gamma} = e \quad (\text{A2})$$

$$a_{WWZ} = \tilde{g}c_{\tilde{\theta}} \left[1 - \frac{x^2}{2C_{\tilde{\theta}}^2} (1 - 2s_{\tilde{\theta}}^4) \right] \quad (\text{A3})$$

$$a_{WWZ_1} = -\frac{\tilde{g}x(1-z^4)}{2\sqrt{2}} \quad (\text{A4})$$

$$a_{WW_1Z} = -\frac{\tilde{g}x(1-z^4)}{2\sqrt{2}c_{\tilde{\theta}}} \quad (\text{A5})$$

$$a_{WW_1Z_1} = -\frac{\tilde{g}}{2} \left[1 - \frac{x^2}{4c_{\tilde{\theta}}^2} \left(1 - (4-z^2) + \frac{z^2}{1-z^2} + \frac{z^2(1+2z^2)c_{2\tilde{\theta}}}{1-z^2} \right) \right] \quad (\text{A6})$$

$$a_{WW_1Z_2} = \frac{\tilde{g}z^2}{2} \left[1 + \frac{x^2z^2}{4c_{\tilde{\theta}}^2} \left(2c_{2\tilde{\theta}} - (4-s_{\tilde{\theta}}^2)z^2 - \frac{2z^2s_{\tilde{\theta}}^2}{1-z^2} \right) \right] \quad (\text{A7})$$

$$a_{WW_2Z_1} = -\frac{z^2\tilde{g}}{2} \left[1 + \frac{x^2}{4c_{\tilde{\theta}}^2} \left(2z^2 - 4z^4c_{\tilde{\theta}}^2 + \left(1 - \frac{2z^4}{1-z^2}s_{\tilde{\theta}}^2 \right) \right) \right] \quad (\text{A8})$$

$$a_{WW_2Z_2} = -\frac{\tilde{g}}{2} \left[1 + \frac{x^2}{4c_{\tilde{\theta}}^2} \left(\frac{1+3z^2(z^2-1+z^4) - s_{\tilde{\theta}}^2(1-3z^2+4z^4+4z^6)}{1-z^2} \right) \right] \quad (\text{A9})$$

$$a_{W_1W_1Z} = -\frac{\tilde{g}c_{2\tilde{\theta}}}{2c_{\tilde{\theta}}} \left[1 + \frac{x^2}{4c_{\tilde{\theta}}^2c_{2\tilde{\theta}}} \left(\frac{3-5z^2-3z^4+z^6}{1-z^2} + s_{\tilde{\theta}}^2 \left(2z^4 + \frac{4z^2}{1-z^2} - 5 - 2c_{2\tilde{\theta}} - c_{4\tilde{\theta}} \right) \right) \right] \quad (\text{A10})$$

$$a_{W_1W_1Z_1} = -\frac{\tilde{g}}{x\sqrt{2}} \left[1 - \frac{x^2}{4c_{\tilde{\theta}}^2} (2c_{\tilde{\theta}}^2 + 1) \right] \quad (\text{A11})$$

$$a_{W_1W_1Z_2} = -\frac{\tilde{g}xz^2(2-z^2+z^2t_{\tilde{\theta}}^2)}{2\sqrt{2}(1-z^2)} \quad (\text{A12})$$

$$a_{W_1W_2Z_2} = \frac{\tilde{g}}{\sqrt{2}x} \left[1 - \frac{x^2}{4c_{\tilde{\theta}}^2} (z^4 + (1+z^4)c_{\tilde{\theta}}^2) \right] \quad (\text{A13})$$

$$a_{W_1W_2Z_1} = \frac{\tilde{g}xz^2 \left(z^2 - 3 + \frac{1}{c_{\tilde{\theta}}^2} \right)}{2\sqrt{2}(1-z^2)} \quad (\text{A14})$$

$$a_{W_1W_2Z} = \frac{z^2\tilde{g}}{2c_{\tilde{\theta}}} \left[1 + \frac{x^2}{4c_{\tilde{\theta}}^2} (2z^2(1-2z^2) + s_{\tilde{\theta}}^2(1+z^4+2c_{2\tilde{\theta}})) \right] \quad (\text{A15})$$

$$a_{W_2W_2Z} = \frac{\tilde{g}c_{2\tilde{\theta}}}{2c_{\tilde{\theta}}^2} \left[1 + \frac{x^2}{4g_1^2c_{\tilde{\theta}}^2c_{2\tilde{\theta}}} \left(4z^2 - 3 - \frac{4z^6c_{\tilde{\theta}}^2}{1-z^2} + (1-z^2)^2s_{\tilde{\theta}}^2 - (2c_{2\tilde{\theta}} + c_{4\tilde{\theta}})s_{\tilde{\theta}}^2 \right) \right] \quad (\text{A16})$$

$$a_{W_2W_2Z_1} = \frac{\tilde{g}}{\sqrt{2}x} \left[1 - \frac{x^2}{4c_{\tilde{\theta}}^2} (1+2z^4c_{\tilde{\theta}}^2) \right] \quad (\text{A17})$$

$$a_{W_2W_2Z_2} = \frac{\tilde{g}x z^4(1 + 2c_{2\tilde{\theta}})}{2\sqrt{2}(1 - z^2)c_{\tilde{\theta}}^2} \quad (\text{A18})$$

All couplings not listed are zero to the order x^2 .

-
- [1] N. Arkani-Hamed, S. Dimopoulos and G. R. Dvali, Phys. Lett. **B429**, 263 (1998), [hep-ph/9803315].
- [2] I. Antoniadis, N. Arkani-Hamed, S. Dimopoulos and G. R. Dvali, Phys. Lett. **B436**, 257 (1998), [hep-ph/9804398].
- [3] L. Randall and R. Sundrum, Phys. Rev. Lett. **83**, 4690 (1999), [hep-th/9906064].
- [4] L. Randall and R. Sundrum, Phys. Rev. Lett. **83**, 3370 (1999), [hep-ph/9905221].
- [5] C. Csaki, C. Grojean, H. Murayama, L. Pilo and J. Terning, Phys. Rev. **D69**, 055006 (2004), [hep-ph/0305237].
- [6] C. Csaki, C. Grojean, L. Pilo and J. Terning, Phys. Rev. Lett. **92**, 101802 (2004), [hep-ph/0308038].
- [7] R. Barbieri, A. Pomarol and R. Rattazzi, Phys. Lett. **B591**, 141 (2004), [hep-ph/0310285].
- [8] G. Cacciapaglia, C. Csaki, C. Grojean and J. Terning, ECONF **C040802**, FRT004 (2004).
- [9] G. Cacciapaglia, C. Csaki, C. Grojean and J. Terning, Phys. Rev. **D70**, 075014 (2004), [hep-ph/0401160].
- [10] R. Sekhar Chivukula, D. A. Dicus and H.-J. He, Phys. Lett. **B525**, 175 (2002), [hep-ph/0111016].
- [11] N. Arkani-Hamed, A. G. Cohen and H. Georgi, Phys. Rev. Lett. **86**, 4757 (2001), [hep-th/0104005].
- [12] N. Arkani-Hamed, A. G. Cohen and H. Georgi, Phys. Lett. **B513**, 232 (2001), [hep-ph/0105239].
- [13] C. T. Hill, S. Pokorski and J. Wang, Phys. Rev. **D64**, 105005 (2001), [hep-th/0104035].
- [14] H.-C. Cheng, C. T. Hill, S. Pokorski and J. Wang, Phys. Rev. **D64**, 065007 (2001), [hep-th/0104179].
- [15] H. Abe, T. Kobayashi, N. Maru and K. Yoshioka, Phys. Rev. **D67**, 045019 (2003), [hep-ph/0205344].
- [16] A. Falkowski and H. D. Kim, JHEP **08**, 052 (2002), [hep-ph/0208058].

- [17] L. Randall, Y. Shadmi and N. Weiner, *JHEP* **01**, 055 (2003), [hep-th/0208120].
- [18] D. T. Son and M. A. Stephanov, *Phys. Rev.* **D69**, 065020 (2004), [hep-ph/0304182].
- [19] J. de Blas, A. Falkowski, M. Perez-Victoria and S. Pokorski, *JHEP* **08**, 061 (2006), [hep-th/0605150].
- [20] G. Cacciapaglia, C. Csaki, C. Grojean and J. Terning, *Phys. Rev.* **D71**, 035015 (2005), [hep-ph/0409126].
- [21] R. Foadi, S. Gopalakrishna and C. Schmidt, *Phys. Lett.* **B606**, 157 (2005), [hep-ph/0409266].
- [22] R. Casalbuoni, S. De Curtis, D. Dolce and D. Dominici, *Phys. Rev.* **D71**, 075015 (2005), [hep-ph/0502209].
- [23] R. Casalbuoni, S. De Curtis, D. Dominici and R. Gatto, *Phys. Lett.* **B155**, 95 (1985).
- [24] R. Casalbuoni, S. De Curtis, D. Dominici and R. Gatto, *Nucl. Phys.* **B282**, 235 (1987).
- [25] A. Birkedal, K. Matchev and M. Perelstein, *Phys. Rev. Lett.* **94**, 191803 (2005), [hep-ph/0412278].
- [26] H.-J. He *et al.*, *Phys. Rev.* **D78**, 031701 (2008), [0708.2588].
- [27] A. Belyaev, 0711.1919.
- [28] A. Alves, O. J. P. Eboli, M. C. Gonzalez-Garcia and J. K. Mizukoshi, *Phys. Rev.* **D79**, 035009 (2009), [0810.1952].
- [29] A. Alves, O. J. P. Eboli, D. Goncalves, M. C. Gonzalez-Garcia and J. K. Mizukoshi, *Phys. Rev.* **D80**, 073011 (2009), [0907.2915].
- [30] E. Accomando, S. De Curtis, D. Dominici and L. Fedeli, *Phys. Rev.* **D79**, 055020 (2009), [0807.5051].
- [31] E. Accomando, S. De Curtis, D. Dominici and L. Fedeli, *Nuovo Cim.* **123B**, 809 (2008), [0807.2951].
- [32] S. De Curtis, *PoS* **2008LHC**, 008 (2008), [1002.2361].
- [33] R. Foadi, S. Gopalakrishna and C. Schmidt, *JHEP* **03**, 042 (2004), [hep-ph/0312324].
- [34] R. Casalbuoni, S. De Curtis and D. Dominici, *Phys. Rev.* **D70**, 055010 (2004), [hep-ph/0405188].
- [35] R. Sekhar Chivukula *et al.*, *Phys. Rev.* **D74**, 075011 (2006), [hep-ph/0607124].
- [36] R. Casalbuoni, S. De Curtis, D. Dominici, F. Feruglio and R. Gatto, *Int. J. Mod. Phys.* **A4**, 1065 (1989).
- [37] R. Barbieri, A. Pomarol, R. Rattazzi and A. Strumia, *Nucl. Phys.* **B703**, 127 (2004),

- [hep-ph/0405040].
- [38] A. Belyaev *et al.*, Phys. Rev. **D79**, 035006 (2009), [0809.0793].
 - [39] L. Basso, A. Belyaev, S. Moretti, G. M. Pruna and C. H. Shepherd-Themistocleous, 1002.3586.
 - [40] CMS Collaboration, G. L. Bayatian *et al.*, preprint CERN-LHCC-2006-001, CMS-TDR-008-1. (2006).
 - [41] ATLAS Collaboration, preprint CERN-LHCC-1999-14, ATLAS-TDR-14. (1999).
 - [42] A. Ballestrero, hep-ph/9911318.
 - [43] A. Ballestrero and E. Maina, Phys. Lett. **B350**, 225 (1995), [hep-ph/9403244].
 - [44] T. Sjostrand, S. Mrenna and P. Skands, JHEP **05**, 026 (2006), [hep-ph/0603175].
 - [45] Particle Data Group, W. M. Yao *et al.*, J. Phys. **G33**, 1 (2006).
 - [46] J. Pumplin *et al.*, JHEP **07**, 012 (2002), [hep-ph/0201195].
 - [47] D0 Collaboration, D0 Note 5923-CONF (2009).
 - [48] S. I. Bityukov and N. V. Krasnikov, Nucl. Instrum. Meth. **A452**, 518 (2000).
 - [49] D0 Collaboration, 1008.2023.